



# A hybrid Eulerian–Lagrangian approach for non-self-similar expansion analysis of a cylindrical cavity in saturated and unsaturated critical state soils

He Yang<sup>1,2</sup> · Pei-Zhi Zhuang<sup>3</sup> · Jia-Liang Zhang<sup>3</sup> · Yue Ma<sup>2</sup> · Hai-Sui Yu<sup>1</sup> · Xiaohui Chen<sup>1,2</sup>

Received: 16 April 2023 / Accepted: 27 November 2023 / Published online: 29 January 2024  
© The Author(s) 2024

## Abstract

This paper proposes a powerful hybrid Eulerian–Lagrangian (HEL) approach for the analysis of cavity expansion problems. The new approach is applied to analysing the non-self-similar expansion process of a hollow cylinder of critical state soils, considering arbitrary saturation states of soils and both drained and undrained conditions. A closed-form solution for the stresses and displacements in the elastic zone is presented, taking the state-dependent soil moduli and outer boundary effect of the soil cylinder into account. Adopting large strain theory in the plastic zone, the non-self-similar cavity expansion process is formulated into a set of partial differential equations in terms of both Eulerian and Lagrangian descriptions, which is solved by a newly proposed algorithm. The HEL approach is compared with the conventional Eulerian and Lagrangian approaches for the cavity expansion analyses. It is found that the new approach can reduce to the Eulerian approach when the self-similar assumption is satisfied and to the Lagrangian approach when stress–total strain relationships are obtained analytically. Finally, the expansion process is proven to be non-self-similar by showing the stress and deformation paths, and the finite thickness of soil cylinders may greatly influence the cavity expansion behaviour, especially with a small thickness ratio. The HEL approach can provide useful tools for validating advanced numerical techniques for both saturated and unsaturated soils and interpreting pressuremeter tests in small-size calibration chambers.

**Keywords** Cavity expansion · Critical state · Hybrid Eulerian–Lagrangian · Finite radial extent · Non-self-similar · Unsaturated soils

## 1 Introduction

Cavity expansion theory studies the distribution and evolution of stresses and deformation around a cylindrical/spherical cavity during continuous expansions, and it

has been increasingly popular in the field of geotechnical engineering since its wide applications such as the interpretation of in situ soil tests [22, 41, 45, 71, 74], capacity prediction of piles, plate anchors and pipelines [25, 30, 43, 60, 80, 82], and stability and deformation analyses of tunnels [35, 75, 79].

---

✉ Xiaohui Chen  
X.Chen@leeds.ac.uk

He Yang  
cnhy@leeds.ac.uk

Pei-Zhi Zhuang  
zhuangpeizhi@sdu.edu.cn

Jia-Liang Zhang  
zhangjiali@mail.sdu.edu.cn

Yue Ma  
cnym@leeds.ac.uk

Hai-Sui Yu  
H.Yu@leeds.ac.uk

<sup>1</sup> School of Civil Engineering, University of Leeds, Leeds LS2 9JT, UK

<sup>2</sup> Geomodelling and AI Centre, School of Civil Engineering, University of Leeds, Leeds LS2 9JT, UK

<sup>3</sup> School of Qilu Transportation, Shandong University, Jinan 250002, China

The quasi-static analysis of cavity expansion generally needs to solve the compatibility equations, stress equilibrium equations, and stress–strain relationships under given boundary conditions. Different assumptions might be made during the analysis [77], for example, small or large strain definitions, drained or undrained conditions, infinite or finite soil mass around the cavity, and various constitutive models of soils. In the past decades, a number of analytical/semi-analytical cavity expansion solutions have been developed, and the solution methods for this typical boundary value problem can be broadly categorised into the so-called auxiliary variable approach (or Eulerian approach) and total strain approach (or Lagrangian approach) [7, 69, 72]. It is worth noting that the Eulerian and Lagrangian approaches defined here are not exactly the same as those usually used in finite element method (FEM) [5]. To make it clear, the so-called Eulerian and Lagrangian approaches here are briefly introduced as follows.

The Eulerian approach highly relies on the self-similar nature of cavity expansion which means that all soil particles go through the same stress and deformation paths [24, 68]. As a result, the incremental stresses and strains related to loading history (i.e. time) and field distribution (i.e. space) are equivalent to each other under a special loading pattern. One branch of this approach, also known as the similarity technique or the incremental velocity method [7, 19, 24, 72, 77], is to transform the PDEs into ordinary differential equation (ODEs) in terms of space (i.e. Eulerian description) by setting the movement of the elastoplastic boundary as the timescale. Another branch formulates the self-similar cavity expansion problem into ODEs in terms of time (i.e. Lagrangian description) by introducing auxiliary variables [14, 57]. Overall, the Eulerian approach is quite powerful and has recently been used to study cavity expansion problems considering anisotropy, structure, viscoplastic, particle crushing, etc. [8, 11, 12, 15, 32, 33, 36, 44, 52, 53, 63, 78]. However, it is not rigorously suitable for the analyses of non-self-similar cavity expansion problems such as the problem investigated in this paper.

The Lagrangian approach can be used in the analyses of both self-similar and non-self-similar cavity expansion problems. This approach normally requires analytical forms of the relationships between stresses and total strains and then relates the current stresses (and strains) to the initial and current radial positions of soil particles. For cavity expansion in perfectly elastoplastic soils under drained conditions, stress fields can be readily known by combining stress equilibrium equations and yield functions, which makes strain fields and particle displacements determined by stress–total strain relationships [2, 9, 29, 73]. Furthermore, for cavity expansion in saturated critical state soils (e.g. Cam Clays) under undrained

conditions, strain fields (and particle displacements) can be readily known due to the constant-volume assumption, and thereby, stress fields can be obtained from the stress–total strain relationships [6, 20, 50, 51, 61, 64, 65, 79]. However, this method has rarely been used in some more complicated conditions since analytical forms of the stress–total strain relationships are often hard to be obtained, for example, analyses in critical state soils under drained conditions.

Previous studies mostly focused on self-similar cavity expansion problems. In fact, solutions for non-self-similar problems are also of great importance, for example, for theoretical analyses of pressuremeter tests and cone penetration tests in small-sized chambers [26, 45, 54, 81], grouting reinforcement problem [28, 31, 66], piezocone tests in partially drained conditions [21, 34, 49], energy piles [23, 39, 76], and reservoir excavation by matrix acidizing [59]. In the analyses of these geotechnical problems, the finite soil thickness and/or thermo-hydro-mechanical-chemical coupling effects determine that the expansion process is no longer self-similar (namely, soil particles at different radial positions do not follow the same stress and deformation paths). In the past some solutions for the expansion analysis of a thick cylinder/sphere of soil have been proposed. For example, using the Lagrangian approach, Yu [69] and Yu [70] derived analytical solutions for the expansion of a hollow thick-wall cylinder and sphere of Mohr–Coulomb soils, respectively, which was extended recently by Zhuang et al. [81] to saturated Cam Clay soils under undrained conditions. For cavity expansion in critical state soils under drained conditions, only a few approximate solutions have also been presented by taking the self-similar-based Eulerian approach [16, 18, 42].

Overall, it is shown that neither the Lagrangian approach nor the Eulerian approach is suitable for the analysis of non-self-similar cavity expansion problems with sophisticated constitutive models and drainage conditions. In order to fill this gap, this paper proposes a new approach, termed as the hybrid Eulerian–Lagrangian (HEL) approach, for non-self-similar cavity expansion problems (e.g. cavity expansion in the bounded soil mass). With the HEL approach, a unified framework is established for the quasi-static expansion analysis of a cylindrical cavity, considering finite/infinite soil mass, drained/undrained conditions, saturated/unsaturated soil states, and various critical state soil models. The novelty of this work lies in two main aspects: (i) an analytical solution for stresses and deformation in the elastic zone is obtained, considering stress-dependent soil modulus of Cam Clay soils and finite cylinder thickness; and (ii) a set of PDEs is established for cavity expansion in the plastic zone with large strain definitions, and it is solved by the HEL approach with high efficiency. The solutions are validated

and discussed by comparing with some existing solutions in special cases such as corresponding self-similar cases, completely dry and fully saturated conditions. Finally, the non-self-similar cavity expansion behaviour in unsaturated soils is highlighted.

## 2 Problem definition and assumptions

The expansion of a hollow thick-wall cylinder of soils upon loading at the inner cavity wall is considered, as shown in Fig. 1. The soil cylinder is of an infinite length (out of plane), and the inner and outer radii of the cylinder are  $a_0$  and  $b_0$ , respectively, at the initial state. A horizontal total stress  $\sigma_{h0}$  and a vertical total stress  $\sigma_{v0}$  act throughout the surrounding soil which is assumed to be isotropic and homogenous. When the inner pressure gradually increases from  $\sigma_{h0}$  to  $\sigma_a$  ( $\sigma_a > \sigma_{h0}$ ), the hollow cylinder will expand outwards with the current inner and outer radii becoming  $a$  and  $b$ , respectively, and the total vertical stress will change from  $\sigma_{v0}$  to  $\sigma_z$ .

Under the geometry and stress boundary conditions defined in Fig. 1, the expansion process can be regarded as an axial-symmetric plane strain problem with respect to the vertical direction. For convenience the problem is investigated in the cylindrical coordinate system  $(r, \theta, z)$  with the origin at the cylinder centre. Taking compression as positive, the stress boundary conditions can be expressed as

$$\sigma_r|_{r=a} = \sigma_a \quad (1)$$

$$\sigma_r|_{r=b} = \sigma_{h0} \quad (2)$$

where  $\sigma_r$  = total radial stress;  $r$  = current radial position of a soil particle.

Neglecting body forces, the stress equilibrium equation in the radial direction is

$$\frac{d\sigma_r}{dr} + \frac{\sigma_r - \sigma_\theta}{r} = 0 \quad (3)$$

where  $\sigma_\theta$  = total circumferential stress; the symbol “d(·)” means the spatial differential of (·) at a given time (i.e. Eulerian description).

The initial saturation state of the surrounding soil is assumed to be arbitrary (e.g. saturated or unsaturated). For a smooth transition of soil state between saturated and unsaturated, the modified Bishop’s definition [3, 4, 46] for the effective (average skeleton) stresses is used as

$$\sigma'_{ij} = \sigma_{ij} - u_a \delta_{ij} + S_r s \delta_{ij} \quad (4)$$

$$s = u_a - u_w \quad (5)$$

where  $\sigma'_{ij}$  = effective stress tensor;  $\sigma_{ij}$  = total stress tensor;  $u_a$  = pore air pressure;  $u_w$  = pore water pressure;  $\delta_{ij}$  = Kronecker’s delta;  $S_r$  = degree of soil saturation;  $s$  = suction stress.  $u_a$  is assumed to equal the atmospheric pressure.

## 3 Critical state model for unsaturated soils

The unsaturated critical state model (UCSM) proposed by Sun et al. [58] is introduced as an example to model the hydro-mechanical behaviour of soils.

### 3.1 Soil water retention curve (SWRC)

SWRC reflects the hydraulic behaviour of unsaturated soils, and it may be affected by the hydraulic hysteresis,

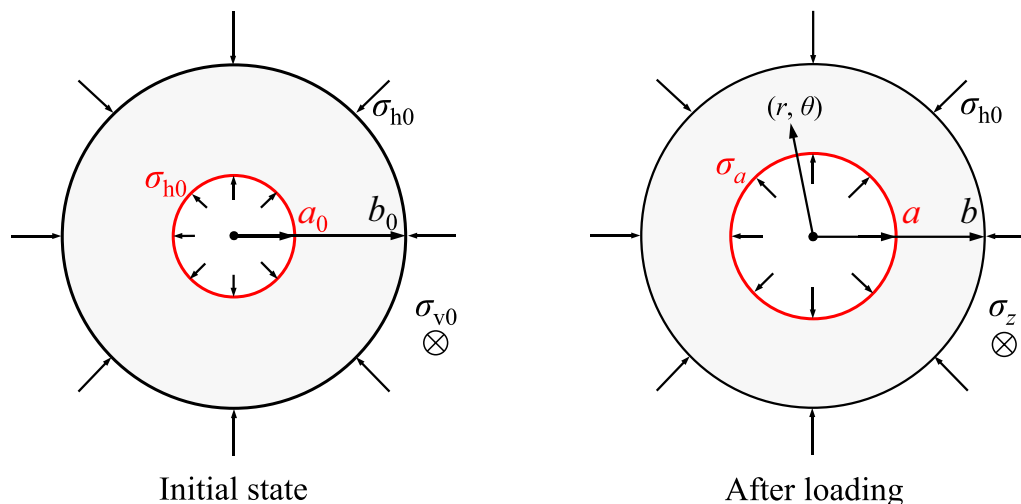


Fig. 1 Expansion of a thick-wall cylinder of soils

pore size distribution, and stress states [27, 38, 47]. A general form of SWRC may be expressed as

$$DS_r = \frac{\partial S_r}{\partial v} Dv + \frac{\partial S_r}{\partial s} Ds \tag{6}$$

where the symbol “D(·)” means the material time differential of (·) for a given soil particle (i.e. Lagrangian description);  $v$  = specific volume.

Taking the expression of Sun et al. [58] as an example, the evolution of  $S_r$  with the suction and volume of soils is defined as

$$DS_r = -\lambda_{se} Dv - (\lambda_{sr}/s) Ds \text{ (for the main drying/wetting curve)} \tag{7}$$

$$DS_r = -\lambda_{se} Dv - (\kappa_{sr}/s) Ds \text{ (for the scanning curve)} \tag{8}$$

where  $\lambda_{se}$  = slope of  $S_r$ - $v$  curve at a constant suction;  $\lambda_{sr}$  and  $\kappa_{sr}$  are the slopes of the main drying/wetting curve and the scanning curve, respectively (see Fig. 2). Under drained conditions (i.e. constant suction) [10], Eq. (6) can be simplified as

$$DS_r = \frac{\partial S_r}{\partial v} Dv \tag{9}$$

Under undrained conditions (i.e. constant water content) [10], the amount of water remains unchanged, which gives

$$\begin{cases} DS_r = -\frac{S_r}{v-1} Dv \\ Ds = \frac{-1}{\partial S_r / \partial s} \left( \frac{S_r}{v-1} + \frac{\partial S_r}{\partial v} \right) Dv \end{cases} \tag{10}$$

It can be summarised that the changes in  $S_r$  and  $s$  can be determined by the change in  $v$  under both drained and undrained conditions. This conclusion will be important for

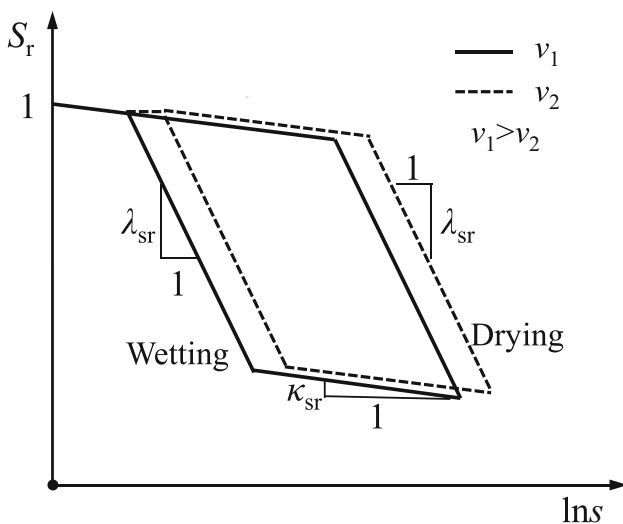


Fig. 2 Void-ratio dependent SWRC

the elastoplastic cavity expansion analysis in Sects. 4 and 5. Moreover, water flow in soils is not considered in this paper in order to develop semi-analytical solutions, and this important phenomenon might be captured by other fully coupled hydro-mechanical numerical methods (e.g. [55, 56]).

### 3.2 Mechanical behaviour

The stress–strain relationship of saturated/unsaturated soils consists of the yield function, plastic potential, hardening law, and elastic behaviour. For typical two-invariant Cam Clay-type critical state models, the loading collapse (LC) yield function  $f$  and plastic potential  $g$  can be expressed, respectively, as

$$f = f[p', q, p'_c(s)] = (\eta/M)^2 - [p'_c(s)/p' - 1] = 0 \tag{11}$$

$$g = g[p', q, p'_g(s)] = 0 \tag{12}$$

where  $f = g$  for the associated plastic flow rule while  $f \neq g$  for the non-associated;  $p' = \sigma'_{ij} \delta_{ij} / 3$  denotes the mean effective stress;  $q = \sqrt{3(\sigma'_{ij} - p' \delta_{ij})(\sigma'_{ij} - p' \delta_{ij})} / 2$  represents the deviatoric stress;  $\eta = q/p'$  is known as the stress ratio;  $M$  = slope of the critical state line (CSL) in the  $p'-q$  plane;  $p'_g(s)$  = size parameter for the plastic potential;  $p'_c(s)$  denotes the isotropic yield stress for unsaturated soils at suction  $s$ , which is the function of the isotropic yield stress for saturated soils ( $p'_c(0)$ ) and the suction:

$$p'_c(s) = \sqrt{3(\sigma'_{ij} - p' \delta_{ij})(\sigma'_{ij} - p' \delta_{ij})} / 2$$

$\left[ \frac{p'_c(s)}{p'_n} \right]^{\lambda(s)-\kappa} = \left[ \frac{p'_c(0)}{p'_n} \right]^{\lambda(0)-\kappa}$  (13)

$$\lambda(s) = \lambda(0)[(1 - \alpha) \exp(-\beta s) + \alpha] \tag{14}$$

where  $p'_n$  = reference stress;  $\lambda(s)$  and  $\lambda(0)$  are the slopes of CSLs in the  $v - \ln p'$  plane at suction  $s$  and 0, respectively;  $\alpha$  and  $\beta$  are material constants for soils in unsaturated states.

The UCSM defines two additional yield surfaces related to the hydraulic behaviour of unsaturated soils, namely the suction-increase yield surface  $f_{SI}$  and suction-decrease yield surface  $f_{SD}$ :

$$\begin{cases} f_{SI} = s - s_I = 0 \\ f_{SD} = s_D - s = 0 \end{cases} \tag{15}$$

where  $s_I$  and  $s_D$  are the suctions controlling the suction-increase and suction-decrease yielding of unsaturated soils, respectively.

The isotropic volumetric hardening law is used to describe the evolution of the yield surface, as

The isotropic volumetric hardening law is used to describe the evolution of the yield surface, as

$$D\varepsilon_v^p = \frac{\lambda(0) - \kappa Dp'_c(0)}{v p'_c(0)} \tag{16}$$

in which  $\varepsilon_v^p$  = plastic volumetric strain;  $\kappa$  = slope of the swelling line in the  $v$ – $\ln p'$  plane and is assumed to be suction-independent [1].

In the elastic loading stage, the volume change can be expressed as

$$\begin{cases} D\varepsilon_v^e = \frac{\kappa}{vp'} Dp' \\ v = v_0 - \kappa \ln(p'/p'_0) \end{cases} \tag{17}$$

where  $\varepsilon_v^e$  = elastic volumetric strain;  $v_0$  = initial specific volume;  $p'_0$  = initial mean effective stress.

### 4 Solutions in the elastic zone

During the elastoplastic expansion process, there will be an elastic zone ( $\rho \leq r \leq b$ ,  $\rho$  denotes the current radius of the elastoplastic boundary) and a plastic zone ( $a \leq r \leq \rho$ ) forming around the cavity. In the elastic zone, the particle displacement is usually small so that the stress–strain relationship can be simplified by the small strain theory:

$$\begin{aligned} \begin{bmatrix} D\varepsilon_r^e \\ D\varepsilon_\theta^e \\ D\varepsilon_z^e \end{bmatrix} &= - \begin{bmatrix} d(Du)/dr \\ Du/r \\ 0 \end{bmatrix} \\ &= \frac{1}{E(v,p')} \begin{bmatrix} 1 & -\mu & -\mu \\ -\mu & 1 & -\mu \\ -\mu & -\mu & 1 \end{bmatrix} \begin{bmatrix} D\sigma'_r \\ D\sigma'_\theta \\ D\sigma'_z \end{bmatrix} \end{aligned} \tag{18}$$

where  $\varepsilon_r^e$ ,  $\varepsilon_\theta^e$ , and  $\varepsilon_z^e$  denote the elastic components of radial, circumferential, and vertical strains;  $u = r - r_0$  is the radial displacement of a soil particle whose initial radial position is  $r_0$ ;  $\mu$  denotes Poisson’s ratio;  $E = 3(1 - 2\mu)vp'/\kappa$  represents the elastic modulus.

#### 4.1 Stress analysis

Before solving Eq. (18), it is necessary to show a conclusion that

$$\begin{cases} \frac{d}{dr} (D\sigma'_r + D\sigma'_\theta) = 0 \\ \frac{d}{dr} [D(S_r s)] = 0 \end{cases} \tag{19}$$

The detailed validation of Eq. (19) is shown in Appendix A. Equation (19) implies that  $(D\sigma'_r + D\sigma'_\theta)$  does not change with the radial position for a given time (but it varies with time). For convenience,  $\sigma'_r + \sigma'_\theta$  can be expressed as

$$\sigma'_r + \sigma'_\theta = 2(\sigma'_h - C_\rho) \tag{20}$$

where  $\sigma'_h$  = effective radial stress at the outer boundary;  $C_\rho$  is a constant determined by the elastoplastic boundary.

Combining Eqs. (3), (18), (19), and (20), the stresses in the elastic zone can be derived as

$$\begin{cases} \sigma'_r = \sigma'_h + C_\rho \left[ (b/r)^2 - 1 \right] \\ \sigma'_\theta = \sigma'_h - C_\rho \left[ (b/r)^2 + 1 \right] \\ \sigma'_z = \sigma'_{v0} + 2\mu(\sigma'_h - \sigma'_{h0} - C_\rho) \end{cases} \tag{21}$$

$$p' = p'_0 + \frac{2}{3}(1 + \mu)(\sigma'_h - \sigma'_{h0} - C_\rho) \tag{22}$$

where  $\sigma'_{h0}$  = effective vertical stress before loading.

The integral constants  $\sigma'_h$  and  $C_\rho$  can be determined by the boundary conditions at  $r = \rho$  and  $r = b$ . Since the total radial stress at  $r = b$  remains unchanged (i.e.  $\sigma_{h0}$ ), combination of Eqs. (2) and (4) gives

$$S_r s - S_{r0} \cdot s_0 = \sigma'_h - \sigma'_{h0} \tag{23}$$

where  $S_{r0}$  = initial degree of saturation and  $s_0$  = initial suction. At the elastoplastic boundary, the stress states ought to be on the initial yield surface so that the initial yield stress  $p'_{c0}(s_0)$  at  $r = \rho$  could be back-calculated from Eq. (11), as

$$p'_{c0}(s_0) = R_0 q_0 f^{-1}(p'_0, q_0) = R_0 p'_0 \left[ 1 + (q_0/Mp'_0)^2 \right] \tag{24}$$

where  $R_0$  = initial overconsolidation ratio of soils;  $q_0$  = initial deviatoric stress.

#### 4.2 Displacement analysis

The incremental form of the radial displacement of a soil particle can be obtained by combining Eqs. (18), (21), and (22) as

$$\begin{aligned} \frac{Du(r)}{r} &= \frac{(1 + \mu)}{E(v,p')} \left( \frac{b}{r} \right)^2 D(\sigma'_h - \sigma'_{h0}) \\ &\quad - \frac{3}{2E(v,p')} \left[ 1 - 2\mu + (b/r)^2 \right] Dp' \end{aligned} \tag{25}$$

Substituting Eqs. (17) and (23) into Eq. (25) and then integrating Eq. (25) following the loading history of a soil particle, the radial displacement becomes

$$\begin{aligned} \frac{u(r)}{r} &= \int_{p'_0}^{p'} \frac{(1 + \mu)\kappa}{3(1 - 2\mu)} \left( \frac{b}{r} \right)^2 \frac{\partial(S_r s)}{\partial p'} \frac{Dp'}{vp'} \\ &\quad + \int_{p'_0}^{p'} \frac{-\kappa \left[ 1 - 2\mu + (b/r)^2 \right]}{2(1 - 2\mu)} \frac{Dp'}{vp'} \end{aligned} \tag{26}$$

As the small strain theory is adopted in the elastic zone, the current radial position of a soil particle can be replaced

by its initial value (i.e.  $r = r_0$ ) in the calculation of elastic displacement. (This assumption can be proved in Sect. 7.1.) Hence, Eq. (26) can be finally integrated as

$$\frac{u(r)}{r} = \frac{(1 + \mu)\kappa}{3(1 - 2\mu)} \left(\frac{b}{r}\right)^2 + \int_{p'_0}^{p'} \frac{\partial(S_r s)}{\partial p'} \frac{Dp'}{vp'} + \frac{1 - 2\mu + (b/r)^2}{2(1 - 2\mu)} \ln\left(1 - \frac{\kappa}{v_0} \ln \frac{p'}{p'_0}\right) \quad (27)$$

The integral of the first term in Eq. (27) mainly depends on the complexity of SWRCs and drained/undrained conditions. The displacements at the elastoplastic boundary and the outer cylinder wall can be computed by Eq. (27) with  $r = \rho$  and  $r = b$ , respectively.

### 4.3 Calculation procedures for the elastic stresses and displacements

The elastic solution for stresses and displacements is much more complex than conventional self-similar cavity expansion problems [10, 14, 19, 37, 67]. The solution also provides the information (i.e. current radius, stresses, and specific volume) at the elastoplastic boundary, which serves as the boundary values for the analysis in the plastic zone. Elastic stresses and displacements can be calculated following the procedure below:

- (i) Input initial parameters, including:  $b_0/a_0, \rho_0; \sigma'_{h0}, \sigma'_{v0}, S_{r0}, s_0, R_0, v_0; \lambda_{sr}, \lambda_{se}, \kappa_{sr}, \kappa, M, s_I, s_D$ ;
- (ii) Calculate  $p'_0$  and  $q_0$  with the initial horizontal and vertical stresses; calculate  $p'_{c0}(s_0)$  by Eq. (24);
- (iii) For a given  $\rho_0$ , set  $p'$  as the basic unknown and substitute Eqs. (9) (or (10), (17), and (21)–(24) into Eq. (11); solve Eq. (11) and obtain  $p'$ ;
- (iv) Then, calculate  $v$  by Eq. (17); calculate  $S_r$  by Eq. (9) for the drained case (or  $S_r$  and  $s$  by Eq. (10) for the undrained case);
- (v) Finally, calculate  $\sigma'_h$  by Eq. (23); calculate  $C_\rho$  by Eq. (22); calculate  $\sigma'_r, \sigma'_\theta,$  and  $\sigma'_z$  by Eq. (21).

## 5 Solutions in the plastic zone

### 5.1 Governing PDEs in the plastic zone

There are five unknowns ( $r, \sigma'_r, \sigma'_\theta, \sigma'_z,$  and  $v$ ) for the analysis in the plastic zone ( $a \leq r < \rho$ ). Five governing equations are established by combining the compatibility equations, the equilibrium equations, the SWRC and stress–strain relationships of soils as follows.

Logarithmic strain definitions are adopted to account for large deformation in the plastic zone, which are expressed as

$$\varepsilon_r = -\ln(dr/dr_0) \quad (28)$$

$$\varepsilon_\theta = -\ln(r/r_0) \quad (29)$$

$$\varepsilon_v = \varepsilon_r + \varepsilon_\theta = -\ln(v/v_0) \quad (30)$$

The compatibility equation in terms of  $r$  and  $v$  can be derived by combining Eqs. (28), (29) and (30) as

$$dr = \frac{vr_0}{v_0 r} dv \quad (31)$$

Substituting the SWRC into the stress equilibrium Eq. (3) gives

$$d\sigma'_r - \frac{\partial(S_r s)}{\partial v} dv = (\sigma'_\theta - \sigma'_r) \frac{dr}{r} \quad (32)$$

For a given soil particle, the incremental form of the stress–strain relationships can be written as

$$\begin{bmatrix} a_{21} & a_{22} & a_{23} & a_{24} \\ a_{31} & a_{32} & a_{33} & a_{34} \\ a_{41} & a_{42} & a_{43} & a_{44} + 1/v \end{bmatrix} \begin{bmatrix} D\sigma'_r \\ D\sigma'_\theta \\ D\sigma'_z \\ Dv \end{bmatrix} = \begin{bmatrix} -Dr/r \\ 0 \\ 0 \end{bmatrix} \quad (33)$$

The derivation of Eq. (33) and related coefficients can be seen in Appendix B.

### 5.2 HEL approach and calculation procedures

Five first-order PDEs are obtained for the analysis in the plastic zone, where Eqs. (31) and (32) are given in the Eulerian description (i.e. for a given time) and Eq. (33) is in the Lagrangian description (i.e. for a given particle). A novel HEL approach is developed to solve the complicated system of PDEs as follows.

The hollow cylinder can be discretised into  $(m-1)$  concentric annuli with  $m$  nodes, while the whole loading process can be discretised into a few load steps. Figure 3 shows the nonlinear distribution of nodes in load step (0) (i.e. before loading), and the radial position of node  $(i)$  satisfies:

$$\begin{cases} r_{(i+1)}^{(0)} = \omega r_{(i)}^{(0)} = \omega^{i-1} a_0 \\ \omega = (b_0/a_0)^{1/(m-1)} \end{cases} \quad (34)$$

where the subscript “ $(i)$ ” ( $i = 1, 2, 3, \dots, m$ ) denotes the node number and the superscript “ $(0)$ ” denotes the load step number.

During the loading process (i.e. the load step increases from (0) to  $(j)$ ), the initial radial position of node  $(i)$  is defined as  $r_{(i)}^{(0)}$  and the current information ( $r, \sigma'_r, \sigma'_\theta, \sigma'_z,$  and

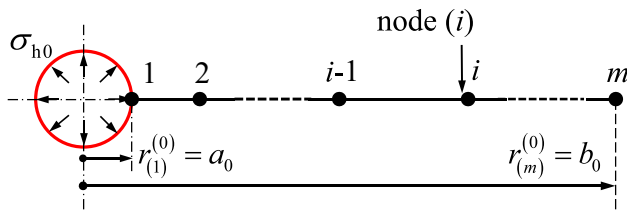


Fig. 3 Definition of nodes before loading

$v$ ) at node  $(i)$  is updated in each step. For convenience, a vector is introduced to store the node information:

$$\mathbf{x}_{(i)}^{(j)} = [r_{(i)}^{(j)}, \sigma'_{r(i)}{}^{(j)}, \sigma'_{\theta(i)}{}^{(j)}, \sigma'_{z(i)}{}^{(j)}, v_{(i)}^{(j)}]^T \tag{35}$$

where the superscript “ $(j)$ ” denotes load step  $(j)$ .

In order to deal with the PDEs, it is defined that the elastoplastic boundary expands to node  $(j)$  at the end of load step  $(j)$  (i.e.  $\rho_0^{(j)} = r_{(j)}^{(0)}$  and  $\rho^{(j)} = r_{(j)}^{(j)}$ ). Consequently, the distribution (along the radial axis at a given time) and evolution (along the time scale of each soil particle) of stresses and displacements can be associated via the elastoplastic boundary, and the change of  $\mathbf{x}_{(i)}^{(j)}$  with nodes and load steps can be seen in Fig. 4. In Fig. 4a, the information vector  $\mathbf{x}_{(i)}^{(j)}$  in the elastic zone (i.e.  $i > j$ ) can be calculated by the elastic solution in Sect. 4, while  $\mathbf{x}_{(i)}^{(j)}$  in the plastic zone (i.e.  $i < j$ ) needs to be computed by solving the governing PDEs. At the elastoplastic boundary,  $\mathbf{x}_{(j)}^{(j)}$  can also be derived by the elastic solution with  $r = \rho_0^{(j)}$ , which serves as the known boundary values for the plastic analysis.

For self-similar cavity expansion problems, the increments of  $\mathbf{x}$  (i.e.  $D\mathbf{x}$  and  $d\mathbf{x}$  in Fig. 4b) can be unified into

either the Eulerian description or the Lagrangian description [14, 19]. Instead, for the present non-self-similar expansion problem, the increments of  $\mathbf{x}$  are solved in the forms of both Eulerian and Lagrangian descriptions in the advanced HEL approach. When the  $(i)$ -th node is loaded from load step  $(j - 1)$  to load step  $(j)$ ,  $D\mathbf{x}$  should be

$$D\mathbf{x} = \mathbf{x}_{(i)}^{(j)} - \mathbf{x}_{(i)}^{(j-1)} \tag{36}$$

On the other hand, in the  $(j)$ -th load step, the increment of  $\mathbf{x}$  from node  $(i + 1)$  to node  $(i)$  is defined as

$$d\mathbf{x} = \mathbf{x}_{(i)}^{(j)} - \mathbf{x}_{(i+1)}^{(j)} = D\mathbf{x} + \mathbf{x}_{(i)}^{(j-1)} - \mathbf{x}_{(i+1)}^{(j)} \tag{37}$$

Combining Eqs. (32), (33), and (37), the PDEs can be transformed into

$$\mathbf{K}[D\sigma'_r, D\sigma'_\theta, D\sigma'_z, Dv]^T = [F_1, F_2, 0, 0]^T \tag{38}$$

where  $\mathbf{K}$ ,  $F_1$ , and  $F_2$  are defined, respectively, as

$$\mathbf{K} = \begin{bmatrix} 1 & 0 & 0 & a_{14} \\ a_{21} & a_{22} & a_{23} & a_{24} \\ a_{31} & a_{32} & a_{33} & a_{34} \\ a_{41} & a_{42} & a_{43} & a_{44} + 1/\nu \end{bmatrix} \tag{39}$$

$$a_{14} = -\frac{\partial(\mathcal{S}_r s)}{\partial v} \tag{40}$$

$$F_1 = (\sigma'_\theta - \sigma'_r) \frac{dr}{r} + \sigma'_{r(i+1)}{}^{(j)} - \sigma'_{r(i)}{}^{(j-1)} + a_{14}(v_{(i+1)}^{(j)} - v_{(i)}^{(j-1)}) \tag{41}$$

$$F_2 = -Dr/r \tag{42}$$

The modified Euler’s method with second-order accuracy is chosen to solve the PDEs (31) and (38), and the procedures are detailed as follows:

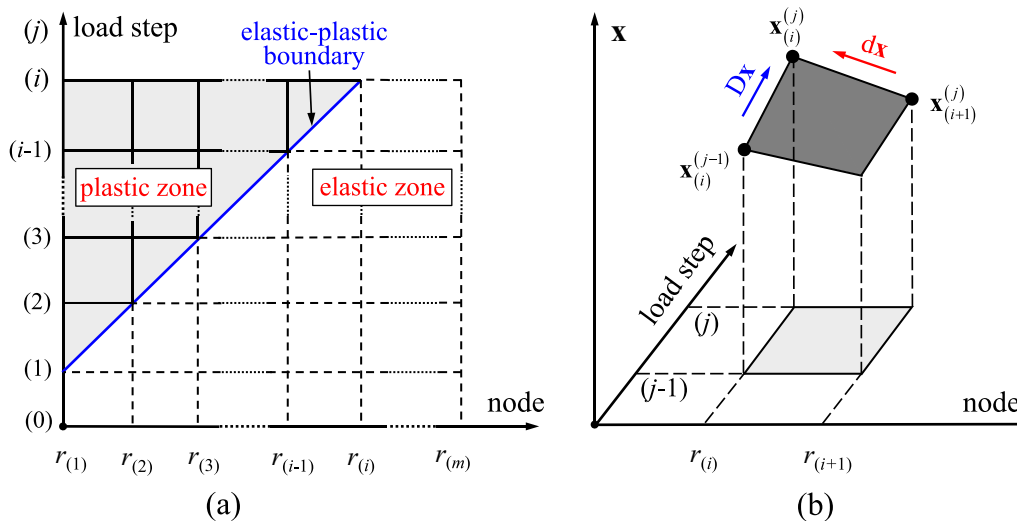


Fig. 4  $\mathbf{x}_{(i)}^{(j)}$  with nodes and load steps: **a** two-dimensional schematic; **b** three-dimensional schematic

- (i) Calculate an approximate value of  $dr$  by Eq. (31) with  $dr_0 = (1 - \omega)r_{(i)}^{(0)}$  and  $\mathbf{x}=\mathbf{x}_{(i+1)}^{(j)}$ ; then calculate approximate  $r_{(i)}^{(j)}$  by  $r_{(i)}^{(j)} = r_{(i+1)}^{(j)} + dr$ ;
- (ii) Calculate  $Dr$  by  $Dr = r_{(i)}^{(j)} - r_{(i)}^{(j-1)}$ ; calculate approximate values of  $[D\sigma'_r, D\sigma'_\theta, D\sigma'_z, Dv]^T$  by Eq. (38) with  $\mathbf{x}=\mathbf{x}_{(i)}^{(j-1)}$  in  $\mathbf{K}$  and  $F_2$ , and  $\mathbf{x}=\mathbf{x}_{(i+1)}^{(j)}$  in  $F_1$ ;
- (iii) Update  $\mathbf{x}=\mathbf{x}_{(i)}^{(j)}$  with  $[D\sigma'_r, D\sigma'_\theta, D\sigma'_z, Dv]^T$  and  $\mathbf{x}_{(i)}^{(j)} = \mathbf{x}_{(i)}^{(j-1)} + D\mathbf{x}$ ;
- (iv) Back-calculate more accurate values of  $\mathbf{x}_{(i)}^{(j)}$  by Eqs. (31) and (38) with  $\mathbf{x}=(\mathbf{x}_{(i)}^{(j-1)} + \mathbf{x}_{(i)}^{(j)})/2$  and  $\mathbf{x}=(\mathbf{x}_{(i)}^{(j)} + \mathbf{x}_{(i+1)}^{(j)})/2$  for those related to the Lagrangian and Eulerian descriptions, respectively;
- (v) In load step ( $j$ ), calculate  $\mathbf{x}_{(i)}^{(j)}$  node-by-node from the elastoplastic boundary to the inner cavity wall (i.e. from  $\mathbf{x}_{(j)}^{(j)}$  to  $\mathbf{x}_{(1)}^{(j)}$ ), and the information of all the nodes in the ( $j$ )-th load step can be determined;
- (vi) Finally, increase the load step from ( $j$ ) to ( $j + 1$ ) and let  $\rho_0^{(j+1)} = r_{(j+1)}^{(0)}$ ; calculate  $\mathbf{x}_{(i)}^{(j+1)}$  node-by-node following procedures (i)-(v). For the whole loading process, gradually increase ( $j$ ) until the inner cavity radius reaches a final value,  $a_{\text{end}}$ .

### 5.3 Analysis in the fully plastic expansion stage

The fully plastic expansion stage, namely the loading-induced plastic zone expands to the outer cylinder wall (i.e.  $\rho_0=b_0$ ), may occur once the thickness of the soil cylinder is finite. In this case, the governing PDEs (31) and (38) still hold, while their boundary values at  $r = \rho$  should be changed to those at  $r = b$ .

For a given  $b$  ( $b > r_{(m)}^{(m)}$ ),  $D(\sigma'_r - S_{r,s})$  remains zero at  $r = b$  since the total radial stress is constant at  $r = b$ . Together with Eq. (33), it gives

$$\mathbf{K}[D\sigma'_r, D\sigma'_\theta, D\sigma'_z, Dv]^T = [0, -Db/b, 0, 0]^T \tag{43}$$

The boundary values at  $r = b$  can be derived from Eq. (43), and  $\mathbf{x}_{(i)}^{(j)}$  can be calculated node-by-node from  $\mathbf{x}_{(m)}^{(j)}$  to  $\mathbf{x}_{(1)}^{(j)}$  following the above procedures.

### 5.4 Comparison of Eulerian, Lagrangian, and HEL approaches

The differences and connections between the proposed HEL approach and other commonly used methods for large strain cavity expansion analysis are compared and discussed as follows.

In the Eulerian approach for self-similar expansion problems (e.g. assume  $b = \infty$  in Fig. 1), the loading history of a particle at  $r = a$  is equivalent to the field distribution from  $r = \infty$  to  $r = a$  due to the self-similarity of stresses and deformation (e.g. Fig. 5a). Therefore, the cavity expansion analysis can be performed by tracing the loading history of a soil particle with auxiliary variables (i.e. path AC) [14, 57], or by focusing on field distributions for a given time with proper timescales (i.e. path BC) [7, 19, 24, 72, 77]. Overall, the information of  $j$  nodes in the plastic zone at the end of ( $j$ )-th load step can be determined via path AC (or BC) due to the self-similarity.

In the Lagrangian approach (see Fig. 5b), the relationship between the effective stress and total strain for node ( $i$ ) should be given analytically to account for path PQ. For drained cavity expansion in Mohr–Coulomb materials, the stress distribution following path MN can be directly calculated by combining the yield function and stress equilibrium equation, and then, the deformation distribution can be obtained with the known stress field and the analytical stress–total strain relationships [9, 69, 70, 73]. Similarly, for cavity expansion in undrained saturated Cam Clay soils, the deformation (or strain) distribution following path MN can be readily determined relying on the constant-volume assumption. Then, the stress distribution can be back-solved from the strain field and the stress–total strain relationships [20, 81].

The HEL approach, in which the PDEs are expressed in the forms of both Eulerian and Lagrangian descriptions and are solved simultaneously (Fig. 4a), is powerful for cavity expansion analysis under various conditions, including drained/undrained conditions, soil cylinder of finite/infinite thickness, saturated/unsaturated state of soils, and various constitutive models. The HEL approach tends to have higher computation efficiency than common numerical methods. For example, when studying drained cavity expansion in critical state soils, Osinov and Cudmani [40] searched the stress fields that satisfy stress boundary conditions and equilibrium equations by multiple iterations and then calculated strain fields node-by-node. This method is relatively time-consuming as it needs to calculate the information of a total of  $m \times j \times \text{iteration}$  times nodes. Comparing to the finite element/difference methods that need to calculate the deformation energies in the whole region (i.e.  $m \times j$  nodes), the HEL approach is also more

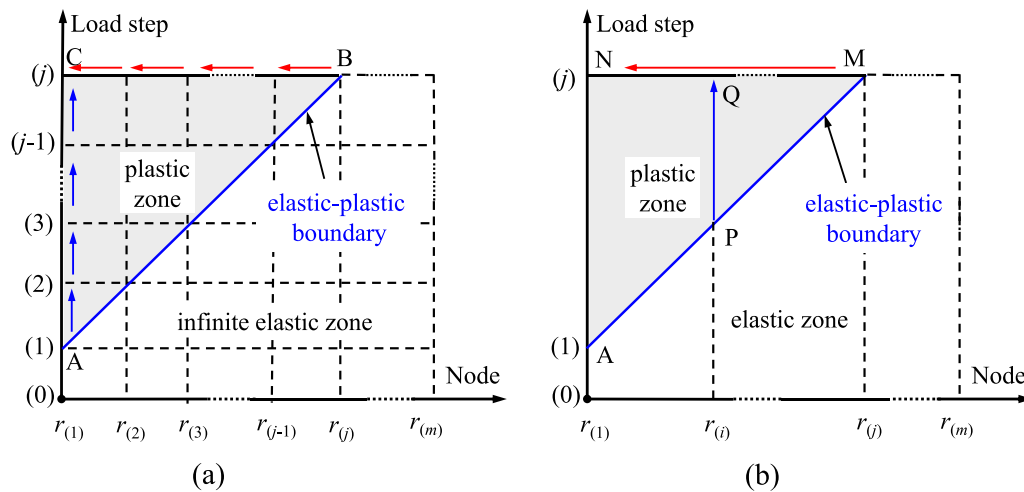


Fig. 5 Schematic of Eulerian and Lagrangian approaches. **a** Eulerian approach; **b** Lagrangian approach

efficient (calculate the information of  $j(j - 1)/2$  nodes) because of the analytical solutions in the elastic zone.

## 6 Special cases

### 6.1 Case 1: self-similar cavity expansion problems

While the thickness of the soil cylinder becomes infinite (i.e.  $b_0/a_0 = \infty$ ), the present problem reduces to the common self-similar cavity expansion problems, and then, the solution can be greatly simplified as follows.

As the internal loading effect vanishes for a particle at  $r = \infty$ , Eq. (44) can be obtained as  $D\sigma'_r + D\sigma'_\theta = 0$  and  $D(S_r s) = 0$ .

$$\sigma'_h - C_\rho = \sigma'_{h0} \tag{44}$$

Then elastic solutions for stresses and deformation can be obtained by substituting Eq. (44) and  $b \rightarrow \infty$  into Eqs. (9), (10), (17), (21), (22), and (25), and this exactly reduces to the solution of Chen et al. [10].

In the self-similar case, the evolution of stresses and strains along the loading history of a soil particle and along the radial direction can be related by  $D\mathbf{x} = d\mathbf{x}$  (but  $Dr \neq dr$  since  $Dr > 0 > dr$ ) [7, 14, 19, 24, 57]. As strains can be fully determined by stresses (Eq. (33)),  $D\mathbf{x} = d\mathbf{x}$  indicates  $D\varepsilon_\theta = d\varepsilon_\theta$ , which gives

$$\frac{Dr}{r} = \frac{dr}{r} - \frac{dr_0}{r_0} \tag{45}$$

Combining Eqs. (31) and (45), a relationship between  $dr$  and  $Dr$  is obtained as

$$\frac{dr}{r} = \frac{1}{1 - (r/r_0)^2 (v_0/v)} \frac{Dr}{r} \tag{46}$$

Substituting Eq. (46) and  $D\mathbf{x} = d\mathbf{x}$  into Eq. (38), we can derive that

$$\mathbf{K} \begin{bmatrix} D\sigma'_r \\ D\sigma'_\theta \\ D\sigma'_z \\ Dv \end{bmatrix} = \frac{Dr}{r} \begin{bmatrix} (\sigma'_\theta - \sigma'_r) \\ 1 - (r/r_0)^2 (v_0/v) \\ -1 \\ 0 \\ 0 \end{bmatrix} \tag{47}$$

The governing PDEs (38) are totally transformed into ODEs (47) in terms of  $Dr/r$  (i.e.  $-D\varepsilon_\theta$ ) with the Lagrangian descriptions, from which  $[D\sigma'_r, D\sigma'_\theta, D\sigma'_z, Dv]^T$  can be readily obtained. Actually, the commonly used auxiliary variables such as  $(r - r_0)/r$ , and  $r_0/r$  [14, 57] are all the derivations of  $\varepsilon_\theta$  and are mainly used to eliminate  $dr/r$  in  $F_1$  (see Eq. (41)). From this point of view, the Eulerian approach is a special case of the HEL approach when  $\ln(r/r_0)$  is chosen as the auxiliary variable and  $b_0/a_0$  becomes infinite.

### 6.2 Case 2: cavity expansions in dry soils ( $S_r = 0$ )

While a cavity expands in ideally dry soils (i.e.  $S_r = 0$ ), the proposed solution can be further simplified as  $\sigma'_{h0} = \sigma'_h$  and  $S_r s = 0$ . Solutions for analysis in the elastic zone can be obtained by substituting  $\sigma'_{h0} = \sigma'_h$  into Eqs. (21), (22), and (27).  $\mathbf{K}$  and  $F_1$  in Eq. (38) for the plastic analysis can be simplified with  $S_r s = 0$  as

$$\mathbf{K} = \begin{bmatrix} 1 & 0 & 0 & 0 \\ a_{21} & a_{22} & a_{23} & 0 \\ a_{31} & a_{32} & a_{33} & 0 \\ a_{41} & a_{42} & a_{43} & 1/v \end{bmatrix} \tag{48}$$

$$F_1 = (\sigma'_\theta - \sigma'_r) \frac{dr}{r} + \sigma'_{r(i+1)} - \sigma'_{r(i)} \tag{49}$$

Combining Eqs. (31), (38), (48), and (49), the node information can be calculated following the same procedures of Sect. 5.2.

### 6.3 Case 3: undrained analysis in fully saturated soils ( $S_r = 1$ )

For cavity expansion in fully saturated soils ( $S_r = 1$ ) under undrained conditions, the specific volume of soils keeps constant (i.e.  $v = v_0$ ) and the suction stress equals the opposite of pore water pressure (i.e.  $s = -u_w$ ). In the elastic zone, the mean effective stress remains unchanged (i.e.  $p' = p'_0$ ), and the stress components, pore water pressure, and displacements can be obtained by substituting Eq. (44) and  $S_r s = -u_w$  into Eqs. (21), (23), and (25). Meanwhile, the PDEs of Eqs. (31)–(33) for the plastic analysis can be simplified with the conditions of  $Dv=0$  and  $du_w = (\partial u_w / \partial v) \cdot dv$ , as

$$dr = \frac{r_0}{r} dr_0 \quad (50)$$

$$d\sigma'_r + du_w = (\sigma'_\theta - \sigma'_r) \frac{dr}{r} \quad (51)$$

$$\begin{bmatrix} a_{21} & a_{22} & a_{23} \\ a_{31} & a_{32} & a_{33} \\ a_{41} & a_{42} & a_{43} \end{bmatrix} \begin{bmatrix} D\sigma'_r \\ D\sigma'_\theta \\ D\sigma'_z \end{bmatrix} = \begin{bmatrix} -Dr/r \\ 0 \\ 0 \end{bmatrix} \quad (52)$$

The new system of PDEs in Eqs. (50)–(52) can be calculated following similar procedures in Sect. 5.2. It is interesting to find that the changes in effective stresses are only related to  $Dr/r$  (see Eq. (52)) and the effective stresses evolve in a self-similar manner even if the cylinder thickness is finite in this special case [81]. It is found that the Lagrangian, Eulerian, and HEL approaches are all suitable for the analysis in this special case, and the advantages and limitations of these approaches will be further discussed in Sect. 7.2.

## 7 Results and discussion

### 7.1 Validation of the HEL approach

The proposed HEL approach is validated at first by comparing with some existing solutions in special cases of saturated and unsaturated soil with an infinite radial extent as follows.

Chen and Abousleiman [13] and Chen and Abousleiman [14] proposed exact solutions for expansion analysis of a cylindrical cavity in an infinite soil mass under ideally undrained and drained conditions, respectively, adopting the modified Cam Clay (MCC) model. As discussed in Sect. 6, these solutions can be regarded as two special

cases of the proposed solution with  $S_r = 1$  and  $S_r(s + u_{w0}) = 0$  ( $u_{w0}$  denotes the initial water pressure), respectively, and  $b_0/a_0 \rightarrow \infty$ . Cavity expansion curves predicted by their solutions and the present solution are compared in Fig. 6, taking the same parameters for Boston Blue clay (i.e. Table 1). In the calculations with the proposed solution,  $b_0/a_0$  is set as 2000 to eliminate the outer boundary effect, and the ideally drained conditions are simulated with  $S_r = 0$  for simplicity. Figure 6 shows that the results calculated by the proposed solution are identical to those published by Chen and Abousleiman [13, 14] in these two typical cases, which proves the accuracy of the proposed HEL approach and the assumption of replacing  $r$  with  $r_0$  in Eq. (27).

Using the Eulerian approach, Chen et al. [10] proposed a solution for cylindrical cavity expansion analysis in infinite unsaturated soils under both drained and undrained conditions. To reproduce the results of Chen et al. [10], the same soil parameters (i.e. Table 2) are used and  $b_0/a_0$  is set as 2000 in the proposed solution. Predicted cavity expansion curves and stress distribution curves at the instant of  $a/a_0 = 2$  for drained and undrained conditions are compared in Figs. 7, 8 and 9. It is shown that the results calculated by the proposed solution agree well with those of Chen et al. [10] while  $b_0/a_0 \rightarrow \infty$ , which further validates the accuracy of the HEL approach. It is also found that the drainage conditions (i.e. constant suction or constant water content) marginally affect the cavity expansion curves. This can be explained by that the coefficients related to drainages conditions (i.e.  $a_{14}$ ,  $a_{24}$ ,  $a_{34}$ , and  $a_{44}$  in Eqs. (38) and (39)) apply minimal influence on  $D\sigma'_k$  ( $k = r, \theta, z$ ) for small changes in  $v$ .

The HEL approach is further validated by comparison with FEM via Abaqus 2020 for cavity expansion in a finite soil mass (e.g.  $b_0/a_0=20$ ). The soils are modelled by the MCC model because it has been well implemented in Abaqus and can be easily recovered from the UCSM by neglecting the suction effect. The numerical simulation model can refer to Zhou et al. [77] with the MCC soil parameters in Table 1, and both the cases of cavity expansion in fully saturated and completely dry soils are compared (i.e.  $S_r = 0$  and 1). Figure 10 shows the cavity expansion curves calculated by the HEL approach and FEM, and identical results can verify the present solution again. These curves in undrained saturated soils are more sensitive to the boundary effect than those in drained dry soils, especially for a higher  $R_0$ . This indicates that the existence of excess water pressure can weaken the boundary effect during the cavity expansion process.

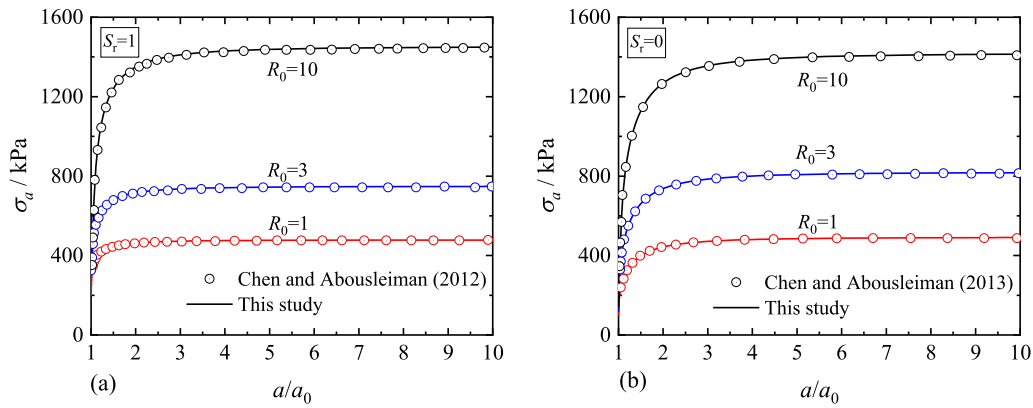


Fig. 6 Comparison of cavity expansion curves: **a** undrained conditions; **b** drained conditions

Table 1 MCC Parameters for Boston Blue clay [13]

$R_0$	$\sigma'_{h0}/\text{kPa}$	$\sigma'_{v0}/\text{kPa}$	$p'_0/\text{kPa}$	$q_0/\text{kPa}$	$\sigma'_{h0}/\sigma'_{v0}$	$\nu_0$
1	100	160	120	60	0.625	2.09
3	120	120	120	0	1	1.97
10	144	72	120	72	2	1.80

$M = 1.2$ ,  $\lambda(0) = 0.15$ ,  $\kappa = 0.03$ ,  $\mu = 0.278$ , and  $\Gamma = 2.74$  (the specific volume at  $p' = 1$  kPa). The initial ambient pore water pressure is 100 kPa for the undrained case

Table 2 UCSM Parameters for unsaturated soils (after Chen et al. [10])

$R_0$	$\sigma'_{h0}/\text{kPa}$	$\sigma'_{v0}/\text{kPa}$	$p_{net0}/\text{kPa}$	$q_0/\text{kPa}$	$\sigma'_{h0}/\sigma'_{v0}$
1	160	220	120	60	0.73
3	180	180	120	0	1
5	190	160	120	30	1.19

$M = 1.2$ ,  $\lambda(0) = 0.15$ ,  $\kappa = 0.03$ ,  $\mu = 0.3$ ,  $\alpha = 0.65$ ,  $\beta = 0.125$ ,  $\lambda_{se} = 0.21$ ,  $\lambda_{sr} = 0.13$ ,  $\kappa_{sr} = 0.13$ ,  $s_I = 120$  kPa,  $s_D = 40$  kPa,  $p'_n = 10$  kPa,  $s_0 = 100$  kPa,  $S_{r0} = 0.6$ ,  $\nu_0 = 2.1$ .  $p_{net0} = p'_0 - S_{r0}s_0$ , which denotes the initial net mean stress

### 7.2 Revisiting undrained cavity expansion in finite, fully saturated soils

Zhuang et al. [81] proposed a semi-analytical solution for undrained analysis of a thick-wall soil cylinder with Cam-Clay soil models, adopting approximate definitions of stress invariants from Collins and Yu [20] (i.e.  $p' = (\sigma'_r + \sigma'_\theta)/2$  and  $q = \sigma'_r - \sigma'_\theta$ ). In order to evaluate the influences of the stress definitions, their solution is compared with the proposed solution that adopts rigorous stress definitions, taking the same soil model (i.e. MCC) and input parameters for London Clay:  $\Gamma = 2.759$ ,

$\lambda(0) = 0.161$ ,  $\kappa = 0.062$ ,  $M = 0.773$ ,  $\nu_0 = 2.0$ ,  $\mu = 0.3$ ,  $a_{end}/a_0 = 4$ , and  $u_{w0} = 0$  [20, 81].

The total cavity pressure  $\sigma_a$  and water pressure  $u_w$  at the inner cavity wall predicted by these two solutions are compared in Figs. 11 and 12 with  $R_0 = 1$  and 16, respectively.  $\sigma_a$  and  $u_w$  calculated by the two solutions vary in the same trend with  $a/a_0$ , while the values predicted by the present solution are mostly larger than those by Zhuang et al. [81]. For example, setting  $a_{end}/a_0 = 4$  and  $b_0/a_0 = 1000$ , the approximate definition of stress invariants leads to 8% and 11% underestimation of the total pressure with  $R_0 = 1$  and 16, respectively. Similar trends were also found by Wang and Chen [65] for cavity expansion in undrained, fully saturated MCC soils of an infinite radial extent. Differences of  $\sigma_a$  between these two solutions become smaller in cases of a smaller  $b_0/a_0$  and a larger  $a/a_0$ . After the peak,  $\sigma_a$  and  $u_w$  predicted by the rigorous solution may decrease faster than those by the approximate one for a small  $b_0/a_0$ . This is due mainly to: (i) when  $b_0/a_0$  is small, the entire soil mass may reach the critical state and  $\sigma_r \rightarrow \sigma_{h0}$  (i.e. confining pressure at  $r = b$ ) [81]; (ii) in the critical state, the effective radial stress in the rigorous solution ( $\sigma'_r = p' + q/\sqrt{3}$ ) is larger than that in the approximate solution ( $\sigma'_r = p' + q/2$ ), so  $u_w$  decreases relatively faster in the rigorous solution.

Figures 13 and 14 plot the effective and total stress paths at the inner cavity wall predicted by the present solution and the solution of Zhuang et al. [81].  $b_0/a_0$  was set as 2 or 1000, and  $a_{end}/a_0 = 4$ . Figure 13 shows that the effective stress paths coincide in all conditions. This is because the deviatoric stress totally depends on the mean effective stress under constant-volume conditions [20, 81], as indicated by Eq. (53).

$$q(p') = Mp' \sqrt{R_0(p'/p'_0)^{-1/\Omega} - 1} \tag{53}$$

where  $\Omega = 1 - \kappa/\lambda(0)$ . On the contrary, the total stress paths obtained by these two solutions are significantly

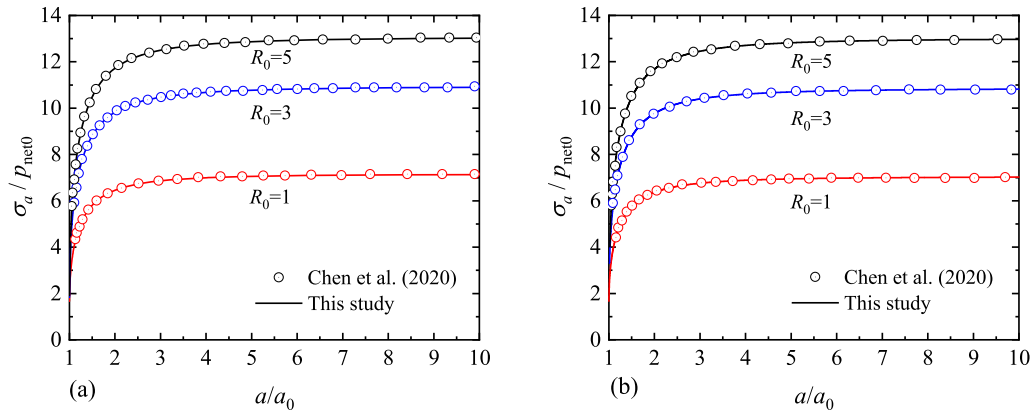


Fig. 7 Comparison of cavity expansion curves with Chen et al. [10] : **a** drained conditions; **b** undrained conditions

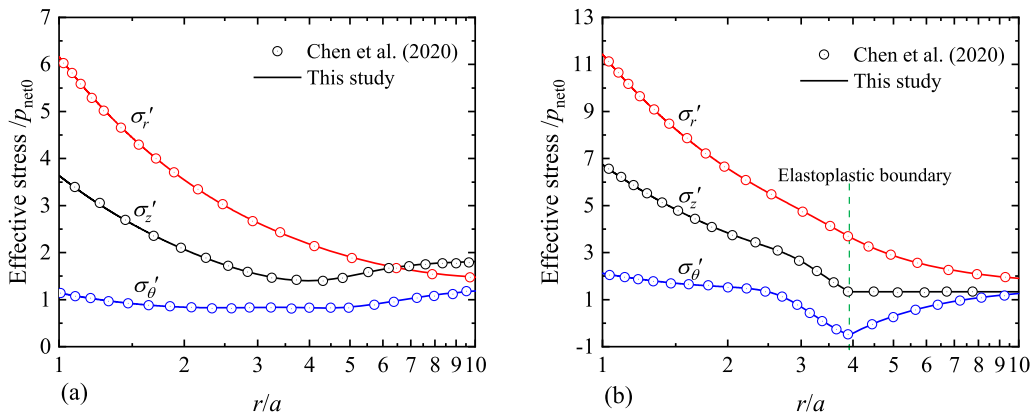


Fig. 8 Comparison of stress distributions with Chen et al. [10] under drained conditions: **a**  $R_0 = 1$ ; **b**  $R_0 = 5$

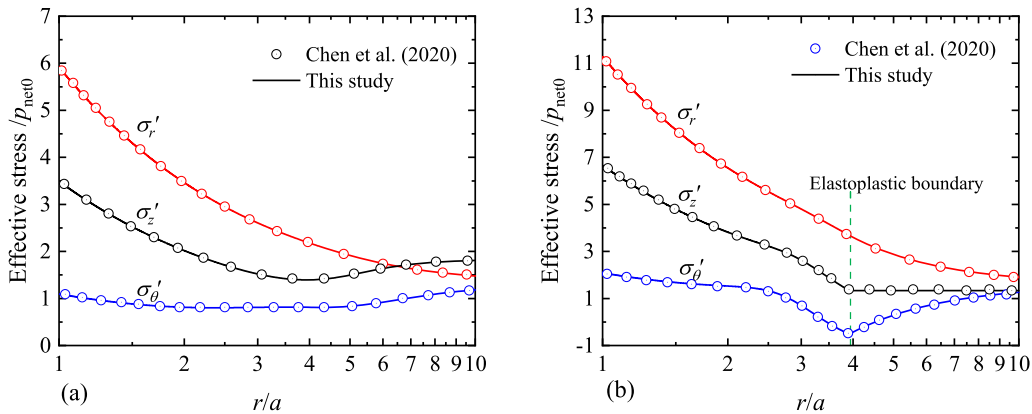


Fig. 9 Comparison of stress distributions with Chen et al. [10] under undrained conditions: **a**  $R_0 = 1$ ; **b**  $R_0 = 5$

different in the normalised  $p$ – $q$  plane ( $p$  denotes the total mean stress) as shown in Fig. 14, and it is explained as follows.

Under the constant-volume conditions ( $D\epsilon_\theta = -D\epsilon_r$ ), Eq. (52) is equivalent to that obtained by Wang and Chen [65] with rigorous stress definitions, which is

$$D\epsilon_\theta = \frac{\kappa}{v_0} \left[ \frac{\sqrt{3}\eta}{M^2 - \eta^2} - \frac{\sqrt{3}(1 + \mu)}{9(1 - 2\mu)} \frac{\partial q}{\partial p'} \right] \frac{Dp'}{p'} \quad (54)$$

With approximate stress invariants, the incremental circumferential strain  $D\tilde{\epsilon}_\theta$  becomes

$$D\tilde{\epsilon}_\theta = \frac{2}{\sqrt{3}} \frac{\kappa}{v_0} \left[ \frac{2\eta}{M^2 - (4/3)\eta^2} - \frac{1}{4(1 - 2\mu)} \frac{\partial q}{\partial p'} \right] \frac{Dp'}{p'} \quad (55)$$

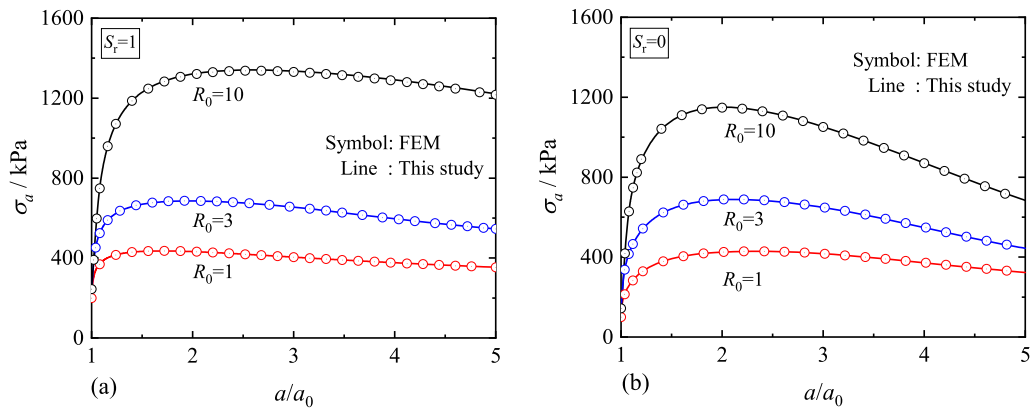


Fig. 10 Comparison of cavity expansion curves: **a** undrained conditions; **b** drained conditions

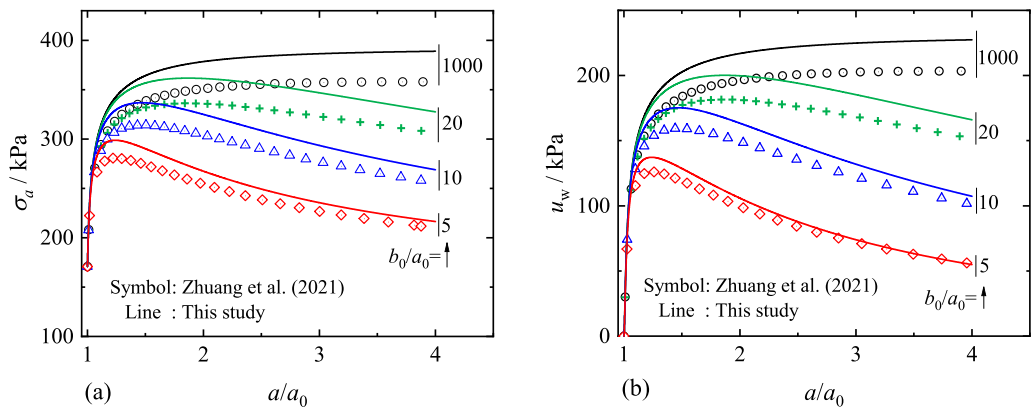


Fig. 11 Cavity expansion response at the inner cavity wall with  $R_0 = 1$ : **a** total cavity pressures; **b** excess water pressures

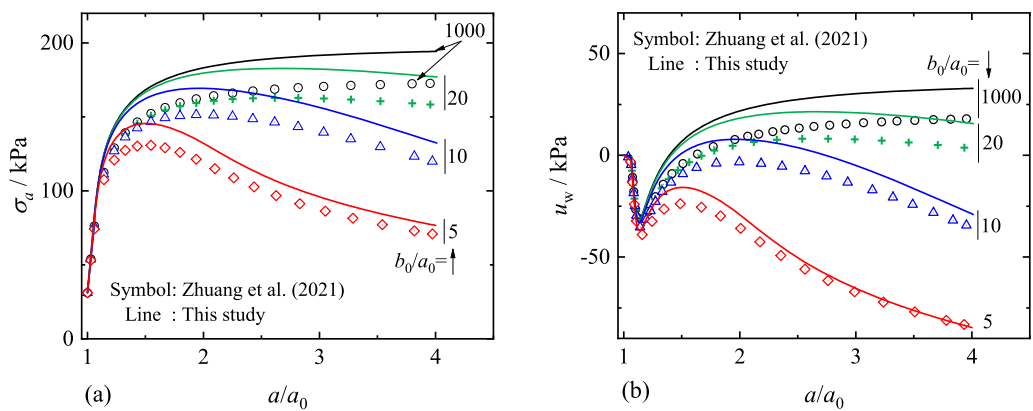


Fig. 12 Cavity expansion response at the inner cavity wall with  $R_0 = 16$ : **a** total cavity pressures; **b** excess water pressures

The difference between Eqs. (54) and (55) results in the different total stress paths with different stress definitions. It also needs to be noted that the stresses (e.g.  $\sigma_a$ ) in Collins and Yu [20] are normalised by the undrained shear strength  $\tilde{s}_u$ , which is different to the standard one  $s_u$  ( $\tilde{s}_u = \sqrt{3}/2s_u \approx 0.866s_u$ ). As a result, the difference between the rigorous and the approximate solutions in the normalised expansion curves was found minimal [48].

Apart from the HEL approach, the applicability of the Eulerian and Lagrangian approaches in this special case is further discussed. Equations (52) and (53) indicate the effective stress paths are self-similar, but the Eulerian approach may still not be applicable because the total stress paths are not self-similar and the outer boundary conditions are difficult to be determined during the fully plastic expansion stage [62]. In addition, is it possible to use the

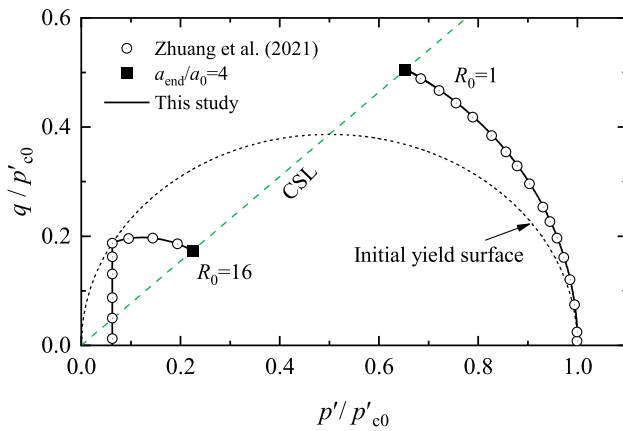


Fig. 13 Effective stress paths at the inner cavity wall

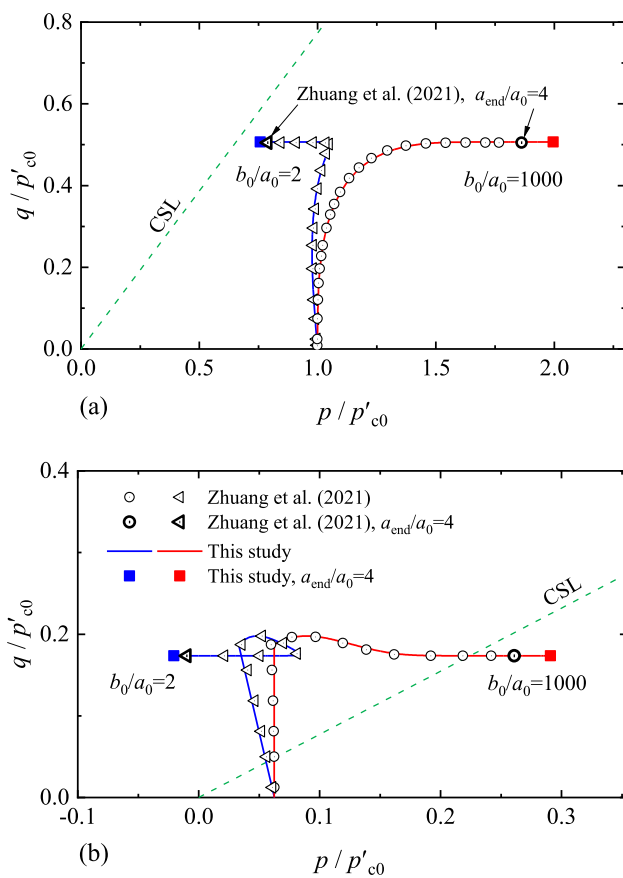


Fig. 14 Total stress paths at the inner cavity wall: **a**  $R_0 = 1$ ; **b**  $R_0 = 16$

Lagrangian approach with rigorous definitions of  $(p', q)$ ? Based on Wang and Chen [65] that solved Eq. (54) by numerical method, this paper goes a step further by integrating Eq. (54) analytically, as

$$\int D\varepsilon_\theta = \frac{\sqrt{3}\kappa}{v_0} \left[ \frac{\Omega}{M} \left( \tan^{-1} \frac{\eta}{M} - \tanh^{-1} \frac{\eta}{M} \right) - \frac{(1 + \mu)}{9(1 - 2\mu)} \left( \eta - 2\Omega\eta + 2M\Omega \tan^{-1} \frac{\eta}{M} \right) \right] \quad (56)$$

Once the analytical stress–total strain relationship is generated, the Lagrangian approach can be readily applied to the analysis of this problem following the same procedures of Zhuang et al. [81].

### 7.3 Cavity expansion behaviour in finite unsaturated soils

The expansion behaviour of a cylindrical cavity in unsaturated soils of a finite radial extent is investigated in this subsection with a particular focus on the finite outer boundary effect and the non-self-similar characteristics. The soil parameters in Table 2 are adopted here, and the analysis is performed only under drained conditions (constant suction) for brevity as similar cavity expansion curves can be expected for undrained analysis (e.g. Figures 7, 8 and 9). The cavity expansion level is up to  $a_{\text{end}}/a_0 = 5$ , and the stresses are normalised by  $p_{\text{net}0} = 120$  kPa.

The pressure–expansion curves and effective stress paths at the inner wall are shown in Figs. 15 and 16 for  $R_0 = 1$  and 5, respectively, with various  $b_0/a_0$  ratios. For the curves with a smaller  $b_0/a_0$ , the inner cavity pressure first increases to reach a peak value and then decreases upon further loading. It proves that the finite cylinder thickness may play an important role in the cavity expansion behaviour, which is consistent with other studies [17, 62, 69, 81]. Different from the expansion behaviour in saturated soils under undrained conditions (see Sect. 7.2), the boundary effect can also influence the effective stress path for unsaturated soils. In Figs. 15b and 16b, the effective stress paths in the  $p'$ - $q$  plot for  $b_0/a_0 = 10$  and 30 turn around after reaching the peak values, which drop along the CSL with  $p'$  and  $q$  reducing, rather than getting steady as that may happen during counterpart cavity expansion analysis with  $b_0/a_0 = \infty$ .

To further highlight the non-self-similar properties, the deformation paths of soil particles at various radial positions are depicted in Fig. 17, taking  $b_0/a_0 = 30$  as an example. It can be seen that soil particles at different radial positions within the soil cylinder take various paths from the initial states to the critical states, which verifies the non-self-similarity nature in the expansion process of thick-wall soil cylinders.

It was mentioned that the self-similar-based Eulerian approach has also been used in the expansion analysis of a cavity in finite critical state soils under drained conditions [16, 18, 42], which are actually approximate solutions as

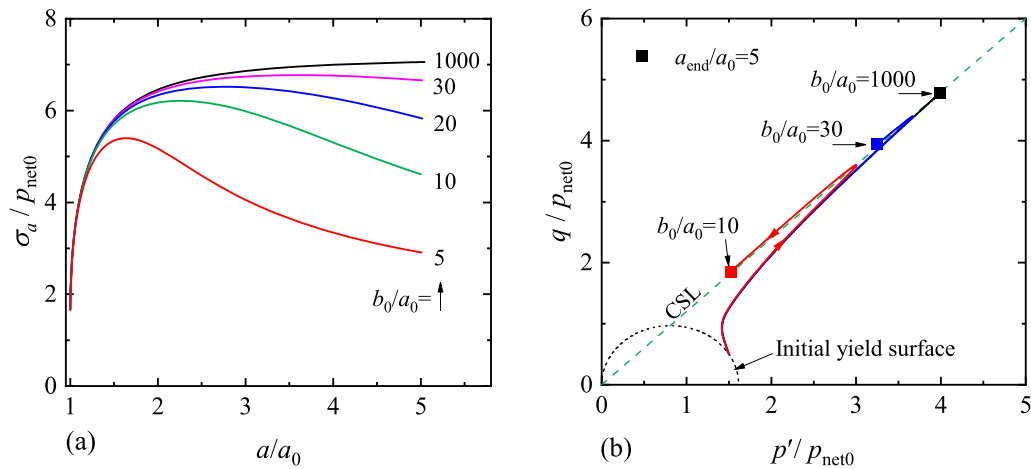


**Fig. 15** Cavity expansion curves and stress paths at the inner cavity wall for  $R_0 = 1$ : **a** cavity expansion curves; **b** stress paths

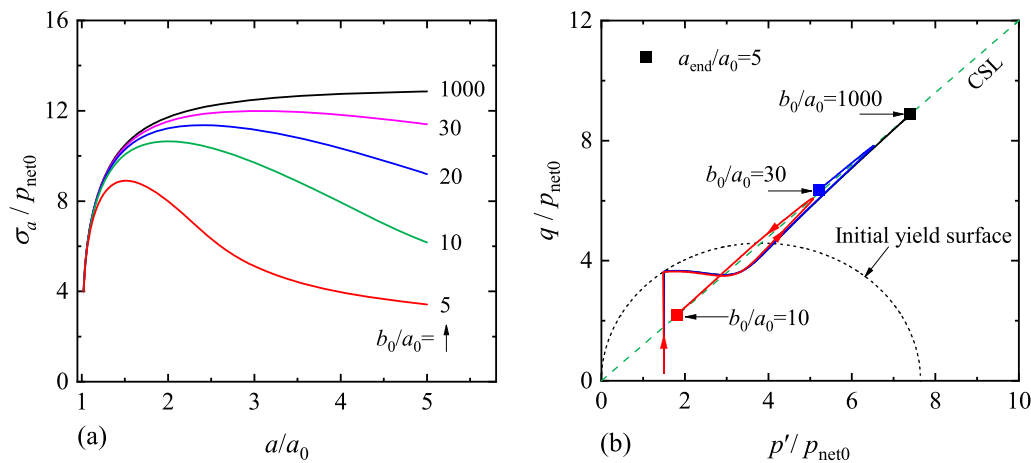


**Fig. 16** Cavity expansion curves and stress paths at the inner cavity wall for  $R_0 = 5$ : **a** cavity expansion curves; **b** stress paths

the expansion proves to be non-self-similar. To highlight the significance of the HEL approach in non-self-similar cavity expansion problems, cavity expansion curves and stress paths at the inner cavity wall are calculated by the HEL approach and the suggested Eulerian approach. The same soil model (i.e. UCSM) and soil parameters (i.e. Table 2) are adopted in the two approaches, and the comparison results are shown in Fig. 18. Two thickness ratios of the cylinder (i.e.  $b_0/a_0 = 10$  and 1000) are selected and  $\rho_0/b_0$  is set as 0.6 in the suggested Eulerian approach in the case of  $b_0/a_0 = 10$ . Not surprisingly, the cavity expansion curves predicted by the two approaches are identical, while  $b_0/a_0$  is large enough (e.g.  $b_0/a_0 = 1000$  in Fig. 18a). However, the predicted pressure–expansion curves vary with each other, while  $b_0/a_0$  is small (e.g.  $b_0/a_0 = 10$ ) as the expansion process is no longer self-similar. In addition,  $\rho_0/b_0$  is assumed as a constant in the suggested Eulerian approach. Consequently, the inner pressure predicted by the Eulerian approach keeps increasing with  $a/a_0$ , which in fact ought to drop after a

peak values as predicted by the present solution. Significant differences are also shown in the stress paths (Fig. 18b), especially in the purely elastic loading process. Hence, considerable errors may be involved by the common Eulerian approach for the expansion analysis of a thick-wall cylinder of soils.

## 8 Conclusions

This paper proposes a novel hybrid Eulerian–Lagrangian (HEL) approach for the expansion analysis of a thick cylinder of soils with arbitrary saturate states under drained or undrained conditions. A closed-form solution for elastic stresses and displacements is developed, considering the finite thickness of the soil cylinder and stress-dependent soil moduli. In the plastic zone, the non-self-similar cavity expansion problem is expressed into five first-order PDEs in terms of both Eulerian and Lagrangian descriptions, and

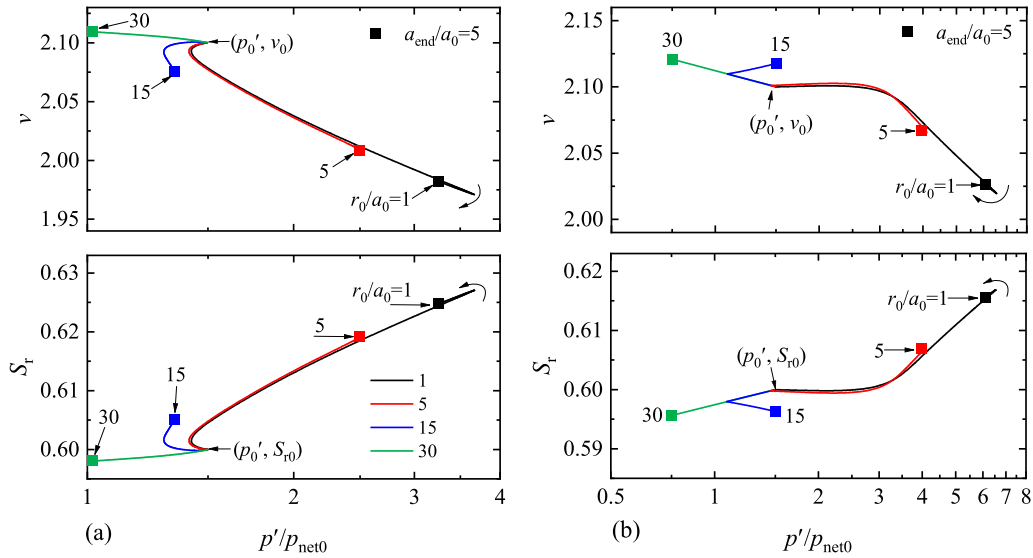


Fig. 17 Deformation paths of various soil particles: **a**  $R_0 = 1$ ; **b**  $R_0 = 5$

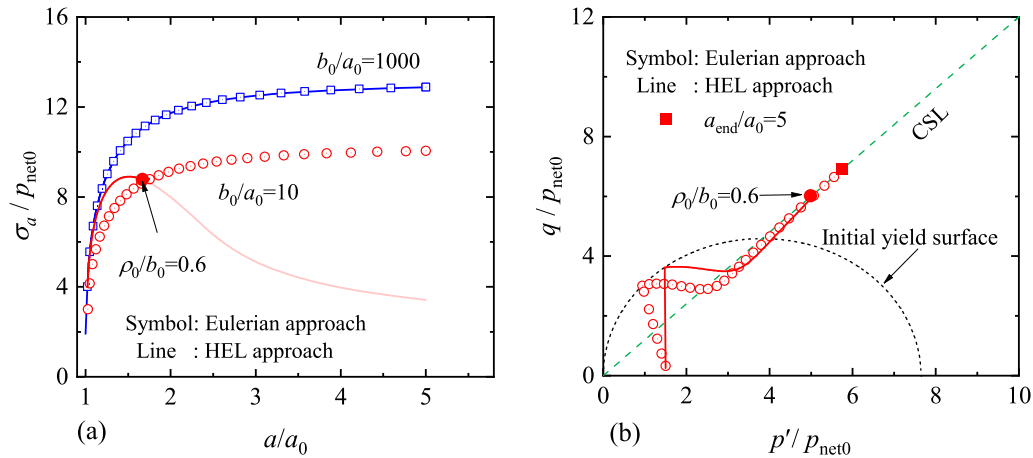


Fig. 18 Cavity expansion curves and stress paths at the inner cavity wall for  $R_0 = 5$ : **a** cavity expansion curves; **b** stress paths

they are solved by a novel algorithm of high efficiency. The following conclusions are drawn:

(i) It proves that the Eulerian approach is a special case of the HEL approach if the cylinder thickness becomes infinite and the Lagrangian approach can be recovered from the HEL approach when the analytical stress–total strain relationship is obtained.

(ii) The commonly used approximate definitions of the stress invariant (i.e.  $p' = (\sigma'_r + \sigma'_\theta)/2$  and  $q = \sigma'_r - \sigma'_\theta$ ) may lead to moderate underestimation of the required expansion pressure in some extreme cases.

(iii) The finite thickness of the soil cylinder may greatly influence the cavity expansion behaviour, which leads to the non-self-similar behaviour during the cavity expansion process. As a result, the self-similar-based Eulerian approach can only provide approximate solutions for this

problem, especially for cylinders with small thickness ratios. The new solutions may provide useful tools for interpreting pressuremeter tests in small-size calibration chambers and also serve as the benchmark for advanced numerical methods for saturated and unsaturated critical state soils. The HEL approach can also provide a general framework for other non-self-similar cavity expansion/contraction problems such as those considering loading/unloading history and thermo-hydro-mechanical-chemical coupling effects.

### Appendix A Validation of Eq. (19)

The validation of Eq. (19) for the stress solution in the elastic zone is shown as follows.

The compatibility equations related to stresses can be derived from Eq. (18) as

$$\frac{d}{dr} [-\mu D\sigma'_r + (1 - \mu)D\sigma'_\theta] + \frac{D\sigma'_\theta - D\sigma'_r}{r} = 0 \tag{57}$$

With the effective stress definition, we can transform the equilibrium equation into

$$\frac{d(D\sigma'_r)}{dr} - \frac{d[D(S_r s)]}{dr} + \frac{D\sigma'_r - D\sigma'_\theta}{r} = 0 \tag{58}$$

Combining Eqs. (57) and (58) gives

$$\frac{d}{dr} [(1 - \mu)(D\sigma'_r + D\sigma'_\theta) - D(S_r s)] = 0 \tag{59}$$

It will be proven that Eq. (59) holds only if when

$$\begin{cases} \frac{d}{dr} (D\sigma'_r + D\sigma'_\theta) = 0 \\ \frac{d}{dr} [D(S_r s)] = 0 \end{cases} \tag{60}$$

As  $D\sigma'_z = \mu(D\sigma'_r + D\sigma'_\theta)$  in plane strain conditions, the mean effective stress satisfies

$$Dp' = \frac{(1 + \mu)(D\sigma'_r + D\sigma'_\theta)}{3} \tag{61}$$

From Eq. (17) the specific volume can be expressed as a function of  $Dp'$  as

$$v = v_0 - \kappa \ln(1 + Dp'/p'_0) \tag{62}$$

Equations (61) and (62) indicate that  $Dv$  is determined by  $(D\sigma'_r + D\sigma'_\theta)$ , and then,  $D(S_r s)$  can also be fully linked by  $(D\sigma'_r + D\sigma'_\theta)$  with the aid of Eqs. (9) and (10). As a result, there will be one basic unknown (i.e.  $D\sigma'_r + D\sigma'_\theta$ ) in Eq. (59). If Eq. (59) always holds during the loading process, we can get that:

$$\frac{d}{dr} (D\sigma'_r + D\sigma'_\theta) = 0 \tag{63}$$

Finally, Eq. (19) can be proved by combining Eqs. (59) and (63).

### Appendix B Derivation of Eq. (33)

In the plastic zone, the stress–strain relationship can be written in the incremental form as

$$De_k^p = \Lambda \frac{\partial g}{\partial \sigma'_k} = \Lambda B_k \tag{64}$$

$$De_v^p = \Lambda \frac{\partial g}{\partial p'} = \Lambda B_p \tag{65}$$

where  $e_k^p$  represents the plastic component of  $\epsilon_k$  ( $k = r, \theta, z$ ); for the UCSM,  $B_k$  and  $B_p$  are specifically expressed as

$$B_k = \frac{M^2 - \eta^2}{3M^2 p'} + \frac{3(\sigma'_k - p')}{M^2 (p')^2}, \quad k = (r, \theta, z) \tag{66}$$

$$B_p = \frac{M^2 - \eta^2}{M^2 p'} \tag{67}$$

$\Lambda$  is a scalar multiplier that can be generally shown as [10]

$$\Lambda = \frac{1}{K_p} (A_r D\sigma'_r + A_\theta D\sigma'_\theta + A_z D\sigma'_z + A_s Ds) \tag{68}$$

where  $A_k$ ,  $A_s$ , and  $K_p$  for the UCSM are:

$$A_k = \frac{\partial f}{\partial \sigma'_k} = \frac{M^2 - \eta^2}{3M^2 p'} + \frac{3(\sigma'_k - p')}{M^2 (p')^2}, \quad k = (r, \theta, z) \tag{69}$$

$$A_s = \frac{\partial f}{\partial s} = -\frac{p'_c(s)}{p'} \lambda(0) \beta (1 - \alpha) e^{-\beta s} \frac{\lambda(0) - \kappa}{[\lambda(s) - \kappa]^2} \ln \left[ \frac{p'_c(0)}{p'_n} \right] \tag{70}$$

$$\begin{aligned} K_p &= -\frac{\partial f}{\partial p'_c(s)} \frac{\partial p'_c(s)}{\partial p'_c(0)} \frac{v p'_c(0)}{\lambda(0) - \kappa} B_p \\ &= \frac{B_p}{p'} \frac{v p'_c(0)}{\lambda(s) - \kappa} \left[ \frac{p'_c(0)}{p'_n} \right]^{\frac{\lambda(0) - \lambda(s)}{\lambda(s) - \kappa}} \end{aligned} \tag{71}$$

Substituting Eq. (68) into Eqs. (64) and (65), the plastic strains can be shown as

$$\begin{bmatrix} De_\theta^p \\ De_z^p \\ De_v^p \end{bmatrix} = \frac{1}{K_p} \begin{bmatrix} A_r B_\theta & A_\theta B_\theta & A_z B_\theta & A_v B_\theta \\ A_r B_z & A_\theta B_z & A_z B_z & A_v B_z \\ A_r B_p & A_\theta B_p & A_z B_p & A_v B_p \end{bmatrix} \begin{bmatrix} D\sigma'_r \\ D\sigma'_\theta \\ D\sigma'_z \\ Dv \end{bmatrix} \tag{72}$$

where

$$A_v = \frac{\partial f}{\partial v} = A_s \frac{\partial s}{\partial v} \tag{73}$$

The total strains are the sum of elastic and plastic strain components, which can be obtained by combining Eqs. (17), (18), and (72):

$$\begin{bmatrix} D\epsilon_\theta \\ D\epsilon_z \\ D\epsilon_v \end{bmatrix} = \begin{bmatrix} a_{21} & a_{22} & a_{23} & a_{24} \\ a_{31} & a_{32} & a_{33} & a_{34} \\ a_{41} & a_{42} & a_{43} & a_{44} \end{bmatrix} \begin{bmatrix} D\sigma'_r \\ D\sigma'_\theta \\ D\sigma'_z \\ Dv \end{bmatrix} \tag{74}$$

where

$$\begin{aligned}
 a_{21} &= \frac{-\mu}{E} + \frac{A_r B_\theta}{K_p}, \\
 a_{22} &= \frac{1}{E} + \frac{A_\theta B_\theta}{K_p}, \\
 a_{23} &= \frac{-\mu}{E} + \frac{A_z B_\theta}{K_p}, \\
 a_{24} &= \frac{A_v B_\theta}{K_p}, \\
 a_{31} &= \frac{-\mu}{E} + \frac{A_r B_z}{K_p}, \\
 a_{32} &= \frac{-\mu}{E} + \frac{A_\theta B_z}{K_p}, \\
 a_{33} &= \frac{1}{E} + \frac{A_z B_z}{K_p}, \\
 a_{34} &= \frac{A_v B_z}{K_p}, \\
 a_{41} &= \frac{1-2\mu}{E} + \frac{A_r B_p}{K_p}, \\
 a_{42} &= \frac{1-2\mu}{E} + \frac{A_\theta B_p}{K_p}, \\
 a_{43} &= \frac{1-2\mu}{E} + \frac{A_z B_p}{K_p}, \\
 a_{44} &= \frac{A_v B_p}{K_p}
 \end{aligned} \tag{75}$$

Finally, by substituting Eqs. (29), (30), and  $D\varepsilon_z = 0$  into Eq. (74), we can obtain Eq. (33):

$$\begin{bmatrix} a_{21} & a_{22} & a_{23} & a_{24} \\ a_{31} & a_{32} & a_{33} & a_{34} \\ a_{41} & a_{42} & a_{43} & a_{44} + 1/\nu \end{bmatrix} \begin{bmatrix} D\sigma'_r \\ D\sigma'_\theta \\ D\sigma'_z \\ Dv \end{bmatrix} = \begin{bmatrix} -Dr/r \\ 0 \\ 0 \end{bmatrix} \tag{76}$$

**Acknowledgements** The first author thanks the financial support from the China Scholarship Council for his study at the University of Leeds. The second authors would like to acknowledge the financial support from the National Natural Science Foundation of China (52108374), the “Taishan” Scholar Program of Shandong Province, China (tsqn201909016), and the Shandong Provincial Natural Science Foundation (ZR202102250562).

## Declarations

**Conflict of interest** The authors have no competing interests to declare that are relevant to the content of this article.

**Open Access** This article is licensed under a Creative Commons Attribution 4.0 International License, which permits use, sharing, adaptation, distribution and reproduction in any medium or format, as long as you give appropriate credit to the original author(s) and the source, provide a link to the Creative Commons licence, and indicate if changes were made. The images or other third party material in this article are included in the article’s Creative Commons licence, unless indicated otherwise in a credit line to the material. If material is not included in the article’s Creative Commons licence and your intended

use is not permitted by statutory regulation or exceeds the permitted use, you will need to obtain permission directly from the copyright holder. To view a copy of this licence, visit <http://creativecommons.org/licenses/by/4.0/>.

## References

- Alonso EE, Gens A, Josa A (1990) A constitutive model for partially saturated soils. *Géotechnique* 40(3):405–430
- Bigoni D, Laudiero F (1989) The quasi-static finite cavity expansion in a non-standard elasto-plastic medium. *Int J Mech Sci* 31(11–12):825–837
- Bishop AW, Blight G (1963) Some aspects of effective stress in saturated and partly saturated soils. *Geotechnique* 13(3):177–197
- Borja RI (2004) Cam-Clay plasticity. Part V: a mathematical framework for three-phase deformation and strain localization analyses of partially saturated porous media. *Comput Methods Appl Mech Eng* 193(48–51):5301–5338
- Borja RI (2013) *Plasticity modeling & computation*. Springer, Berlin-Heidelberg
- Cao LF, Teh CI, Chang MF (2001) Undrained cavity expansion in modified Cam clay. *Géotechnique* 51(4):323–334
- Carter JP, Yu H-S (2022) Cavity expansion in cohesive-frictional soils with limited dilation. *Géotechnique* 73(7):629–635
- Castro J, Sivasithamparan N (2022) Theoretical solution for drained cylindrical cavity expansion in clays with fabric anisotropy and structure. *Acta Geotech* 17(5):1917–1933
- Chadwick P (1959) The quasi-static expansion of a spherical cavity in metals and ideal soils. *Q J Mech Appl Math* 12(1):52–71
- Chen H, Li L, Li J (2020) Elastoplastic solutions for cylindrical cavity expansion in unsaturated soils. *Comput Geotech* 123:103569
- Chen H, Mo P-Q (2022) An undrained expansion solution of cylindrical cavity in SANICLAY for K0-consolidated clays. *J Rock Mech Geotech Eng* 14(3):922–935
- Chen S, Abousleiman Y, Muraleetharan KK (2022) Computational implementation of bounding surface model and its verification through cavity benchmark problems. *Int J Numer Anal Methods Geomech* 46(3):553–569
- Chen SL, Abousleiman YN (2012) Exact undrained elasto-plastic solution for cylindrical cavity expansion in modified Ca Clay soil. *Géotechnique* 62(5):447–456
- Chen SL, Abousleiman YN (2013) Exact drained solution for cylindrical cavity expansion in modified Cam Clay soil. *Géotechnique* 63(6):510–517
- Cheng W, Chen RP, Pereira JM, Cui YJ (2022) Undrained cylindrical cavity expansion/contraction in stiff clays using a two-surface plasticity model. *Int J Numer Anal Methods Geomech* 46(3):570–593
- Cheng Y, Yang H-W, Sun DA (2018) Cavity expansion in unsaturated soils of finite radial extent. *Comput Geotech* 102:216–228
- Cheng Y, Yang H, Xu Z, Lu C (2022) Cavity expansion analysis of normal indentation of rocks with lateral confinement. *Comput Geotech* 145:104693
- Cheng Y, Yang HW (2019) Exact solution for drained spherical cavity expansion in saturated soils of finite radial extent. *Int J Numer Anal Methods Geomech* 43(8):1594–1611
- Collins IF, Pender MJ, Wang Y (1992) Cavity expansion in sands under drained loading conditions. *Int J Numer Anal Methods Geomech* 16(1):3–23
- Collins IF, Yu H-S (1996) Undrained cavity expansions in critical state soils. *Int J Numer Anal Methods Geomech* 20(7):489–516

21. Dienstmann G, Maghous S, Schnaid F (2017) Theoretical analysis and finite-element simulation for nonlinear poroelastic behavior of cylinder expansion in infinite media under transient pore-fluid flow conditions. *Int J Geomech* 17(7):04017001
22. Fu Y, Ma C, Bian Y, Lv G, Hu Y, Wang C (2022) Stochastic mechanics-based Bayesian method calibrating the constitutive parameters of the unified model for clay and sand with CPTU data. *Acta Geotech* 17(10):4577–4598
23. Gaaloul I, Montassar S, Frikha W (2021) Thermal effects on limit pressure in a cylindrical cavity expansion. *Innov Infrastruct Solut* 6:1–11
24. Hill R (1950) *The mathematical theory of plasticity*. Oxford University Press, London, UK
25. Jardine R, Zhu B, Foray P, Yang Z (2013) Interpretation of stress measurements made around closed-ended displacement piles in sand. *Géotechnique* 63(8):613–627
26. Jewell RJ, Fahey M, Wroth CP (1980) Laboratory studies of the pressuremeter test in sand. *Geotechnique* 30(4):507–531
27. Khalili N, Romero E, Marinho FA (2022) State of the art report. *Advances in unsaturated soil mechanics: constitutive modelling, experimental investigation, and field instrumentation*. In proceedings of the 20th ICSMGE-state of the art and invited lectures. Rahman and Jaks, Sydney, Australia, p 297–348
28. Kumar JS, Chaudhuri A, Detournay E, Kandasami RK (2023) Fluid injection-induced cavity expansion in dry porous medium. *Int J Numer Anal Methods Geomech* 48:104–122. <https://doi.org/10.1002/nag.3631>
29. Li C, Ym S (2022) Large-strain analysis for cylindrical cavity contraction in strain-softening geomaterials. *Int J Numer Anal Methods Geomech* 46(16):3012–3027
30. Li L, Li J, Da S, Gong W (2017) Semi-analytical approach for time-dependent load–settlement response of a jacked pile in clay strata. *Can Geotech J* 54(12):1682–1692
31. Liu H, Zhou H, Kong G, Qin H, Zha Y (2017) High pressure jet-grouting column installation effect in soft soil: theoretical model and field application. *Comput Geotech* 88:74–94
32. Liu H, Zhou H, Wang Z, Li X (2021) Theoretical solution for cavity expansion in crushable soil. *Int J Geomech* 21(7):04021098
33. Liu K, Chen S (2019) Analysis of cylindrical cavity expansion in anisotropic critical state soils under drained conditions. *Can Geotech J* 56(5):675–686
34. Mafra V, Dienstmann G (2022) Cavity expansion solutions applied to help assess the partial drainage behavior characterization of the piezocone test. *Comput Geotech* 152:105017
35. Mair RJ, Taylor RN (1993) Prediction of clay behaviour around tunnels using plasticity solutions. In *predictive soil mechanics: proceedings of the wroth memorial symposium*. Thomas Telford, Oxford, UK
36. Mo P-Q, Chen H, Yu H-S (2022) Undrained cavity expansion in anisotropic soils with isotropic and frictional destructuration. *Acta Geotech* 17(6):2325–2346
37. Mo P-Q, Yu H-S (2018) Drained cavity expansion analysis with a unified state parameter model for clay and sand. *Can Geotech J* 55(7):1029–1040
38. Ng CWW, Zhou C, Chiu CF (2020) Constitutive modelling of state-dependent behaviour of unsaturated soils: an overview. *Acta Geotech* 15(10):2705–2725
39. Olgun CG, Ozudogru TY, Arson C (2014) Thermo-mechanical radial expansion of heat exchanger piles and possible effects on contact pressures at pile–soil interface. *Geotechn Lett* 4:170–178
40. Osinov VA, Cudmani R (2001) Theoretical investigation of the cavity expansion problem based on a hypoplasticity model. *Int J Numer Anal Methods Geomech* 25(5):473–495
41. Patino-Ramirez F, Wang ZJ, Chau DH, Arson C (2023) Back-calculation of soil parameters from displacement-controlled cavity expansion under geostatic stress by FEM and machine learning. *Acta Geotech* 18(4):1755–1768
42. Pournaghiazar M, Russell AR, Khalili N (2013) Drained cavity expansions in soils of finite radial extent subjected to two boundary conditions. *Int J Numer Anal Methods Geomech* 37(4):331–352
43. Randolph MF, Dolwin R, Beck R (1994) Design of driven piles in sand. *Geotechnique* 44(3):427–448
44. Russell AR, Khalili N (2006) On the problem of cavity expansion in unsaturated soils. *Comput Mech* 37(4):311–330
45. Salgado R, Mitchell JK, Jamiolkowski M (1997) Cavity expansion and penetration resistance in sand. *J Geotech Geoenviron Eng* 123(4):344–354
46. Schrefler B (1984) *The finite element method in soil consolidation*. University College of Swansea
47. Sheng D (2011) Review of fundamental principles in modelling unsaturated soil behaviour. *Comput Geotech* 38(6):757–776
48. Sheng D, Sloan SW, Yu H-S (2000) Aspects of finite element implementation of critical state models. *Comput Mech* 26(2):185–196
49. Silva MF, White DJ, Bolton MD (2006) An analytical study of the effect of penetration rate on piezocone tests in clay. *Int J Numer Anal Methods Geomech* 30(6):501–527
50. Silvestri V, Abou-Samra G (2011) Application of the exact constitutive relationship of modified Cam clay to the undrained expansion of a spherical cavity. *Int J Numer Anal Methods Geomech* 35(1):53–66
51. Silvestri V, Abou-Samra G (2012) Analytical solution for undrained plane strain expansion of a cylindrical cavity in modified cam clay. *Geomech Eng* 4(1):19–37
52. Silvestri V, Tabib C (2018) Application of cylindrical cavity expansion in MCC model to a sensitive clay under  $K_0$  consolidation. *J Mater Civ Eng* 30(8):04018155
53. Sivasithamparam N, Castro J (2020) Undrained cylindrical cavity expansion in clays with fabric anisotropy and structure: theoretical solution. *Comput Geotech* 120:103386
54. Song X-G, Yang H, Yue H-Y, Guo X, Yu H-S, Zhuang P-Z (2022) Closed-form solutions for large strain analysis of cavity contraction in a bounded Mohr-Coulomb medium. *Eur J Environ Civ Eng* 26(10):4548–4575
55. Song X, Borja RI (2014) Finite deformation and fluid flow in unsaturated soils with random heterogeneity. *Vadose Zone J*. <https://doi.org/10.2136/vzj2013.07.0131>
56. Song X, Borja RI (2014) Mathematical framework for unsaturated flow in the finite deformation range. *Int J Numer Methods Eng* 97(9):658–682
57. Su D (2021) Drained solution for cylindrical cavity expansion in modified Cam Clay soil under constant vertical stress. *Can Geotech J* 58(2):176–189
58. Sun Da, Sheng D, Sloan SW (2007) Elastoplastic modelling of hydraulic and stress–strain behaviour of unsaturated soils. *Mech Mater* 39(3):212–221
59. Tang X, Hu M (2022) A reactive-chemo-mechanical model for weak acid-assisted cavity expansion in carbonate rocks. *Rock Mech Rock Eng* 56:515–533
60. Vesic AS (1972) Expansion of cavities in infinite soil mass. *J Soil Mech Found Div* 98(SM3):265–290
61. Vrakas A (2016) A rigorous semi-analytical solution for undrained cylindrical cavity expansion in critical state soils. *Int J Numer Anal Methods Geomech* 40(15):2137–2160
62. Wang C-I, Zhou H, Liu H-I, Ding X-m (2022) Analysis of undrained spherical cavity expansion in modified Cam Clay of finite radial extent. *Eur J Environ Civ Eng* 26(3):952–963
63. Wang H, Li L, Li J (2022) A numerical investigation on undrained expansion of a cylindrical cavity under biaxial in situ

- stresses using anisotropic S-CLAY1 model. *Int J Numer Anal Methods Geomech* 46(18):3402–3424
64. Wang X, Chen S-L, Zhang JJ (2023) A graphical solution for undrained cylindrical cavity expansion in strain-hardening frictional soil. *Acta Geotech* 18:1–14
  65. Wang X, Chen S (2022) Revisiting undrained cavity expansion problem in critical state soils: a simple graph-based approach. *Int J Numer Anal Methods Geomech* 46(12):2356–2374
  66. Wang Z-F, Shen S, Modoni G, Zhou A (2020) Excess pore water pressure caused by the installation of jet grouting columns in clay. *Comput Geotech* 125:103667
  67. Yang C, Li J, Li L, Da S (2021) Expansion responses of a cylindrical cavity in overconsolidated unsaturated soils: a semi-analytical elastoplastic solution. *Comput Geotech* 130:103922
  68. Yang H, Yu H-S, Chen X, Zhuang P-Z (2023) Rigorous solution for drained analysis of spherical cavity expansion in soils of finite radial extent. *Comput Geotech* 160:105516
  69. Yu H-S (1992) Expansion of a thick cylinder of soils. *Comput Geotech* 14(1):21–41
  70. Yu H-S (1993) Finite elastoplastic deformation of an internally pressurized hollow sphere. *Acta Mech Solida Sinica* 6(1):81–97
  71. Yu H-S (1994) State parameter from self-boring pressuremeter tests in sand. *J Geotech Eng* 120(12):2118–2135
  72. Yu H-S, Carter JP (2002) Rigorous similarity solutions for cavity expansion in cohesive-frictional soils. *Int J Geomech* 2(2):233–258
  73. Yu H-S, Houlsby GT (1991) Finite cavity expansion in dilatant soils: loading analysis. *Géotechnique* 41(2):173–183
  74. Yu H-S, Mitchell JK (1998) Analysis of cone resistance: review of methods. *J Geotech Geoenviron Eng* 124(2):140–149
  75. Yu H-S, Rowe RK (1999) Plasticity solutions for soil behaviour around contracting cavities and tunnels. *Int J Numer Anal Methods Geomech* 23(12):1245–1279
  76. Zhou H, Kong G, Liu H, Laloui L (2018) Similarity solution for cavity expansion in thermoplastic soil. *Int J Numer Anal Methods Geomech* 42(2):274–294
  77. Zhou H, Liu H, Wang Z, Ding X (2021) A unified and rigorous solution for quasi-static cylindrical cavity expansion in plasticity constitutive models. *Comput Geotech* 135:104162
  78. Zhou H, Wang Z, Liu H, Shen H, Ding X (2021) Undrained cylindrical and spherical cavity expansion in elastic-viscoplastic soils. *Can Geotech J* 58(10):1543–1557
  79. Zhuang P-Z, Yang H, Yue H-Y, Fuentes R, Yu H-S (2022) Plasticity solutions for ground deformation prediction of shallow tunnels in undrained clay. *Tunn Undergr Space Technol* 120:104277
  80. Zhuang P-Z, Yu H-S (2018) Uplift resistance of horizontal strip anchors in sand: a cavity expansion approach. *Géotechn Lett* 8(4):284–289
  81. Zhuang P-Z, Yu H-S, Mooney SJ, Mo P-Q (2021) Loading and unloading of a thick-walled cylinder of critical-state soils: large strain analysis with applications. *Acta Geotech* 16:237–261
  82. Zhuang P-Z, Yue H-Y, Song X-G, Yang H, Yu H-S (2021) Uplift behavior of pipes and strip plate anchors in sand. *J Geotech Geoenviron Eng* 147(11):04021126

**Publisher's Note** Springer Nature remains neutral with regard to jurisdictional claims in published maps and institutional affiliations.